Doctoral Dissertation

Studies on Synthesis of Rare Earth Phosphors and Their Application to LED Solid Illumination

（希土類蛍光体の合成とLED固体照明への応用に関する研究）

Hyo Sung Kim

February 2015

Division of Applied Chemistry

Graduate School of Engineering

Osaka University

Preface

The presented studies of this thesis were performed under the supervision of Professor Ken-ichi Machida at Division of Applied Chemistry, Graduate School of Engineering of Osaka University during years 2010-2015.

White light emitting diodes (LEDs) have brought a revolution in the fields of illuminations and displays. The objective of this thesis was to synthesize the efficient long-wavelength emitting nitride phosphors for the white LEDs. Several novel and efficient synthesis processes were developed and the resultant products showed excellent photoluminescence properties.

The author hopes that the results and findings obtained in the present studies will contribute to the researches for optical materials and their applications, and further development to the related academic and industrial researches.

Hyo Sung Kim

Materials Chemistry
Graduate School of Engineering
Osaka University
Yamada-oka, Suita, Osaka 565-0871
Japan

February, 2015

Contents

General Introduction

1. Application of white LEDs

Recently, white light emitting diodes (LEDs) have been paid much attention because of their low energy-consumption, long service lifetime, and quick response. They are widely used in many fields such as LED lamps general lighting, backlight units for liquid-crystal displays, and so on [1]. Figure 1 (a) shows the percentage of application of the LEDs in 2012. The applications as the backlight units for cellular phones, TV and general lighting constitute large percentages. The luminous efficiency for the light output of white LEDs is much increased only within few years and their prices are also going down compared with other types of lamps. In consequence of developing of white LEDs' fabrication techniques, it is predicted that the luminous efficiency of LED chips will exceed 150 lm/W in the coming future, that is much higher than the conventional incandescent lamps.

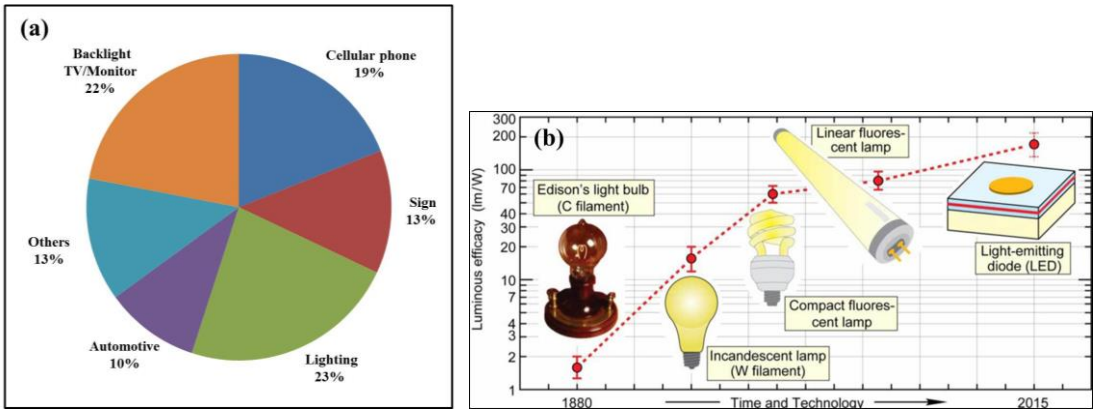

Fig. 1. (a) The percentage of application fields of the LED lamps and backlights produced all over the world in 2012, and (b) the annual profiles of luminous efficiency for main lights parts.

2. Fabrication of white LEDs

In the LED-related technology, methods for creating a white light are roughly classified to three types: (i) A primitive type using three individual LED chips with green, blue, and red color components; (ii) a hybrid type of near UV-LED combined with blue, green, and red phosphors; and (iii) the other hybrid type of a blue LED combined with yellow or green and red phosphors [2]. The first type has the basic design that red, blue, and green LED chips are fabricated to be

adjacent to one another, and colors and intensity of lights emitted from three chips are controlled to generate such white lights. This type of white color is generally produced by using such red, green, and blue LEDs (GaAsP, GaP, InGaN/AlGaN double hetero structure). However, thermal quenching characteristics of each LED chip are different from one another and it is hard for us to create an uniform color mixing state.

As a result, the research works made up to date are mainly focused on the second or third type of white LEDs as called phosphor-converted (pc) white LEDs. The source of first light emitted from the near UV or blue-LED chips and the color of second light of which the wavelength is converted by the fluorescent substance are mixed, so that the white light output is realized (see Fig. 2). For example, most conventional way to generate white light emission is to combine the InGaN blue emitting LED with a Ce^{3+}-doped yttrium aluminum garnet (YAG) yellow phosphor [3]. For application in illumination or some other fields, this type can simply provide the white light output. However, such white-light output has limited the correlated color temperature (CCT) ranging from 5000 to 11000 K, so that is called "cold-white light" [4,5]. Also, this model has low CRI (Color Rendering Index) value due to the lack of color of green and red color components. As the substitutions for lamps, lower CCT ranging, high CRI value is required to the use for illumination lighting markets. So, the longer wavelength-emitting phosphors that can be efficiently excited by the emission of GaN or InGaN LED chip are urgently required.

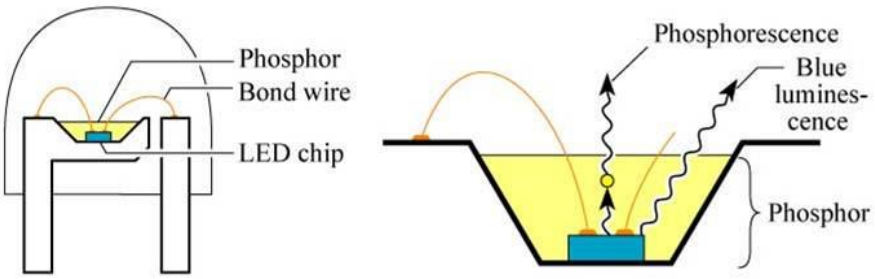

Fig. 2. Schematic illustrations of phosphor-converted white LEDs.

3. Nitride phosphors for white LEDs

Other than the nitride phosphors, some phosphors such as orthosilicates [6,7], aluminates [8], and sulfides [8,9] have also been used for white LEDs. However, since most of oxidic phosphors

only have low absorbability in the visible light region this makes them impossible to be coupled with blue LED. On the other hand, sulfidic phosphors are thermally unstable and very sensitive to moisture, so that their emission intensity is degraded significantly in ambient atmosphere without a protective coating layer. Consequently, to solve these problems and develop high-performance phosphors for white LEDs, it is essential to improve the present phosphors or to explore new host materials for the phosphors. Compared with these oxidic or sulfidic phosphors, the nitride phosphors have excellent emission intensity, color rendering, chemical stability, and thermal quenching property. The nitrogen atoms in such nitride host lattices are generally connected with two ($N^{[2]}$) or three ($N^{[3]}$) silicon atoms, even four ($N^{[4]}$), for the phosphors such in $BaYbSi_4N_7$ [10], and $BaSi_7N_{10}$ [11]. The degree of condensation κ (simply defined as the molar ratio of Si/N) has been observed within a range of 1/2–3/4, which is not accessible for oxysilicates (the maximum is 1/2 in SiO_2) [12]. So, the nitride phosphors are chemically and thermally stable due to the highly condensed SiN_4-based networks.

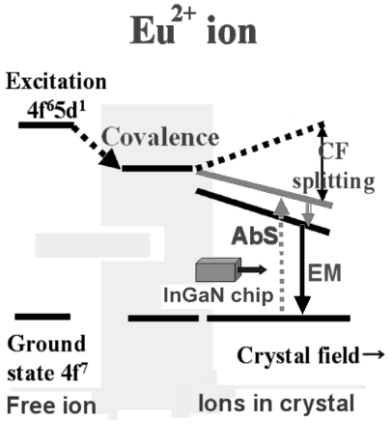

Fig. 3. Emission of Eu^{2+} in crystals.

Our research group has succeeded in producing high quality $M^{II}_2Si_5N_8:Eu^{2+}$ (M^{II} = Ca, Sr, Ba) [13,14] and $CaAlSiN_3:Eu^{2+}$ [15] phosphors which have practically been used as key materials for high color-rendering solid illumination parts based on blue-emitting InGaN chips as the red color component source since the 5*d* energy level for the excited state of Eu^{2+} ion is effectively lowered by "nephelauxetic effect" (see Fig. 3) of the Eu-N bonding with a covalence character and the 4f electron of Eu^{2+} ion is excited to the 5*d* energy level even by the blue light of LED chip.

In order to produce these excellent nitride phosphors, much efficient nitriding procedure and high active starting materials are strongly required. Until now, only a few preparation routes are developed for these nitride phosphors, for example, the conventional solid-state reaction, *viz*. $(1-x)/3Ca_3N_2 + x\text{EuN} + \text{AlN} + 1/3Si_3N_4 + N_2 \rightarrow CaAlSiN_3:Eu^{2+}$. However, Ca_3N_2 is moisture sensitive. Also, high temperature and pressure are necessary to complete the nitriding reactions. Therefore, new synthesis processes are strongly required for producing the high-quality nitride phosphors.

3. Purpose and scope of this work

To solve the above-mentioned problems on the nitride phosphors, $CaAlSiN_3:Eu^{2+}$ and $(Sr,Ca)AlSiN_3:Eu^{2+}$, the present study was carried out to aim the following points:

I. To develop new convenient and practical synthesis processes to produce the high-quality nitride phosphors.

II. To characterized the photoluminescence properties of the resultant phosphors at the practical use level.

III. To improve the brightness of the nitride phosphors compared with the $YAG:Ce^{3+}$ standard phosphor.

This thesis consists of four chapters excluding the general introduction part:

Chapter 1 describes the direct nitridation process of $MAlSiN_3:Eu^{2+}$ (M = Ca, Sr) phosphor by using fine metal hydride powders. The phase composition and particle morphology analyses are performed to carry out to confirm the quality of the resultant phosphors. The photoluminescence properties are characterized for the practical use as the white LEDs. The flux effect of CaH_2 on the emission intensity is systematically investigated for the $CaAlSiN_3:Eu^{2+}$ and $(Sr,Ca)AlSiN_3:Eu^{2+}$ phosphors.

In Chapter 2, molecular organic acid salts, *e.g.* $Ca(CH_3COO)_2$ are used as a calcium source to produce the $CaAlSiN_3:Eu^{2+}$ phosphor, and the luminescence properties are characterized to aim the practical use of these as the white LEDs. The high-quality phosphorous powders are obtained

from the $Ca(CH_3COO)_2$-based starting materials that show high emission intensity and good stability against the thermal quenching effect.

Chapter 3 describes the developed carbothermal reduction and nitriding process using $CaCN_2$ as a dual-roled reagent of calcium source and reductant. By optimizing the molar ratio between Ca and Al elements for the starting materials: $CaCN_2$, $CaCO_3$:Eu^{2+}, AlN, and Si_3N_4, the high-quality powder of $CaAlSiN_3$ phosphor are produced by a flux effect of $CaCN_2$.

Chapter 4 summarizes the results and conclusions obtained in the whole work.

References

[1] S. Nakamura, T. Mukai, M. Senoh, *Appl. Phys. Lett.*, **64** (1994**)** 1687.

[2] U. Kaufmann, M. Kunzer, K. Kohler, H. Obloh, W. Pletschen, P. Schlotter, J. Wagner, A. Ellens, W. Rossner, M. Kobusch, *Phys. Stat. Sol. A.*, **192** (2002) 246.

[3] *English Translation of Japanese Patent Application*, **No. 245381** Filed Sep. 18, 1996, Nichia Chemical Industries Ltd.

[4] M. L. Badgutdinov, E. V. Korobov, F. A. Luk'yanov, A. E. Yunovich, L. M. Kogan, N. A. Gal'china, I. T. Rassokhin, N. P. Soshchin, *Semiconductors*, **40** (2006) 739.

[5] Y. Narukawa, I. Niki, K. Izuno, M. Yamada, Y. Murazaki, T. Mukai, *Jpn. J. Appl. Phys.*, **41** (2002) L371.

[6] J. K. Park, C. H. Kim, S. H. H. D. Park, S. Y. Park, *Appl. Phys.Lett.*, **84** (2004) 1647.

[7] J. K. Park, K. J. Choi, J. H. Yeon, S .J. Lee, C. H. Kim, *Appl. Phys.Lett.*, **88** (2006) 043511.

[8] D. Jia, D. N. Hunter, *J. Appl. Phys.*, **100** (2006) 113125.

[9] Y. R. Do, K. Y. Ko, S. H. Na, Y. D. Huh, *J. Electrochem. Soc.*, **153** (2006) H142.

[10] Y. Q. Li, G. de With, H. T. Hintzen, *J. Alloys Compd.*, **385** (2004**)** 1.

[11] H. Huppertz, W. Schnick, *Chem. Eur. J.*, **3** (1997) 249.

[12] H. A. Hoeppe, F. Stadler, O. Oeckler, W. Schnick, Angew. *Chem. Int. Ed.*, **43** (2004**)** 5540.

[13] X. Piao, T. Horikawa, H. Hanzawa, K. Machida, *Appl. Phys.Lett.*, **88** (2006) 161908.

[14] X. Piao, K. Machida, T. Horikawa, H. Hanzawa, *Appl. Phys.Lett.*, **91** (2007) 041908.

[15] X. Piao, K. Machida, T. Horikawa, H. Hanzawa, Y. Shimomura, N. Kijima, *Chem. Mater.*, **19** (2007) 4592.

Chapter 1

Luminescence Properties of $CaAlSiN_3:Eu^{2+}$ and $(Sr,Ca)AlSiN_3:Eu^{2+}$ Phosphors Prepared by Direct-nitriding Method using Fine Metal Hydride Powders

In this chapter, a convenient and mass scale synthesis route, direct nitridation method is developed to prepare the quaternary nitride $MAlSiN_3$ (M=Sr, Ca) solid solution by using M-Al-Si-Eu (M=Sr, Ca) alloy and hydride M-Al-Si-Eu (M=Sr, Ca) alloy powders as precursors. The hydride process was very useful to decrease alloy particle size below 20 μm and such small sized particle well reacted even under the normal pressure of N_2 gas. This work also provides an easy route to synthesize nitride compounds without using any sensitive raw materials under normal pressure. As the excited state of Eu^{2+} ($4f^6 5d$) is strongly influenced by the crystal field strength [1-10], another goal of this work is to realize the fine emission color tuning of Eu^{2+} ion in the series of $MAlSiN_3$ (M=Ca, Sr) host through their solid solution formation.

1.1 $CaAlSiN_3:Eu^{2+}$ phosphor

1.1.1 Introduction

For a conventional method to produce the $CaAlSiN_3:Eu^{2+}$ phosphor, metal nitrides of Ca_3N_2, AlN, Si_3N_4, and EuN are used as the starting materials and severe conditions (*e.g.* 0.9 MPa, 1800°C) are inevitably applied to them [11]. However, this procedure has the following problems: 1) A few of the metal nitrides used for the raw materials (Ca_3N_2 and EuN) are chemically unstable (deliquescent), so that this is responsible for the oxygen impurity to lower the emission intensity of the resultant phosphors. 2) The high pressure and temperature conditions must be required to produce the $CaAlSiN_3:Eu^{2+}$ phosphor.

Meanwhile, the $CaAlSiN_3:Eu^{2+}$ phosphors have been tried to produce directly from the corresponding Ca-Eu-Al-Si intermetallic compound, (Ca,Eu)AlSi [12], where CaAlSi is well known as a superconducting material with Tc = 7.8 K [13]. However, the resultant nitrides still contain the metal residue and thus, any high-quality $CaAlSiN_3:Eu^{2+}$ phosphor has hardly been produced by this direct-nitriding method.

It is well known that some metals react with hydrogen to form brittle metal hydrides, which are easily pulverized to fine powders ("hydrogen embrittlement"). Since these hydride powders are highly reactive, the present authors have synthesized $M_2Si_5N_8:Ce^{3+}$ (M=Ca, Sr, Ba) phosphors by the direct-nitriding method using an appropriate mixture of $MSiH_x$, Si_3N_4, and CeF_3 as the starting materials [14], so that good luminescence properties are observed on them.

In this work, the $CaAlSiN_3:Eu^{2+}$ phosphors were synthesized from the starting materials mixing the $(Ca,Eu)AlSiH_x$ powder derived from the (Ca,Eu)AlSi intermetallic compound with various amounts of CaH_2 powder added as a flux, where the mean particle size of (Ca,Eu)AlSi powder was below 20 μm to be fine enough for absorbing hydrogen and the resultant hydride powder is so reactive with N_2 that it is easily converted to the nitride phase. The resultant $CaAlSiN_3:Eu^{2+}$ phosphors were characterized to meet the requirements of the red light source used as white LEDs.

1.1.2 Experimental Section

An intermetallic compound, (Ca,Eu)AlSi, was prepared from Ca (99.0%, Wako), Al (99.99%, Nilaco), Si (99.9999%, Koujundo Kagaku), and Eu (99.5%) metal ingot by the conventional arc-melting method in an Ar gas.

Generally, 3 at% of Eu atom to the total amount of Ca one was doped to prepare the intermetallic compound, $(Ca_{0.97}Eu_{0.03})AlSi$, where the weight loss of Eu metal was evaluated to be less than 1 wt% during the arc-melting process. The resultant ingots were brittle enough to grind finely on an agate mortar in a glove box filled with the purified Ar gas which was maintained oxygen and moisture concentrations below several ppm. The obtained (Ca,Eu)AlSi powder was heated in a H_2 gas at 3.0 MPa and 450^{o}C for 1 h and then was ground again in the same way in the glove box. The resultant $(Ca,Eu)AlSiH_x$ powder was transferred to a BN crucible, and then loaded into a radio frequency (RF) furnace equipped with the ZrB_2 heater which was located in a zirconia crucible with Si_3N_4 balls. The heating chamber was pumped down and back filled with an high purity N_2 (6N) gas, and heated under a continuous N_2 flow with a rate of 20 ml/min. The temperature was slowly (10°C/min) increased up to 1050°C, at which the Self-propagating High-temperature Synthesis (SHS) reaction occurred [15], and then the sample

was heated again at 1500°C for 6 h for further nitridation. After heating, the power was switched off and the product was cooled down to room temperature in the chamber of electric furnace. In order to remove impurity phases formed as a by products, the powders of $CaAlSiN_3:Eu^{2+}$(3 at%) phosphor were washed with a 1N HCl aqueous solution for a few minutes and furthermore, they were washed again with water. Finally, these powders were dried at 100°C for several hours in air.

1.1.3 Result and Discussion

Fig. 1-1 shows typical XRD patterns of the (Ca,Eu)AlSi and (Ca,Eu)$AlSiH_x$ powders used as the raw materials for the $CaAlSiN_3:Eu^{2+}$ phosphor. The observed reflection peaks were well assigned according to cell data (hexagonal, S.G. = P6/MMM, a = 4.220(2), c = 4.422(5), c/a = 1.047(7)) reported elsewhere on the intermetallic compound of CaAlSi [12,13] although CaSi peaks (around $2\theta = 32^o$, 39^o) derived from CaSi phase were still detected on the samples, suggesting that 3 at% of Eu metal was ununiformly doped in the CaAlSi crystal lattice to form the $(Ca_{0.97}Eu_{0.03})AlSi$ solid solutions. The oxygen content of as-obtained (Ca,Eu)AlSi and hydrogenated (Ca,Eu)$AlSiH_x$ powders was well suppressed below about 0.5 wt%. This oxygen contaminant was possibly originated from the Ca metal ingot used for preparing the intermetallic compound of (Ca,Eu)AlSi because the surface parts of Ca ingot pieces were usually oxidized.

The XRD pattern of (Ca,Eu)$AlSiH_x$ powder is shown in Fig. 1-1 (b). Since most of the reflection peaks recorded are also assigned based on the similar crystal lattice to that of CaAlSi, one can see that the resultant metal hydride is uniformly hydrogenated without any decomposition to the another metals or metal hydride phases. The evaluated lattice constants and cell volume are listed in the Table 1-1. By treating with hydrogen, all of these values were increased, suggesting that the crystal lattice of (Ca,Eu)$AlSiH_x$ was expanded compared with that of (Ca,Eu)AlSi.

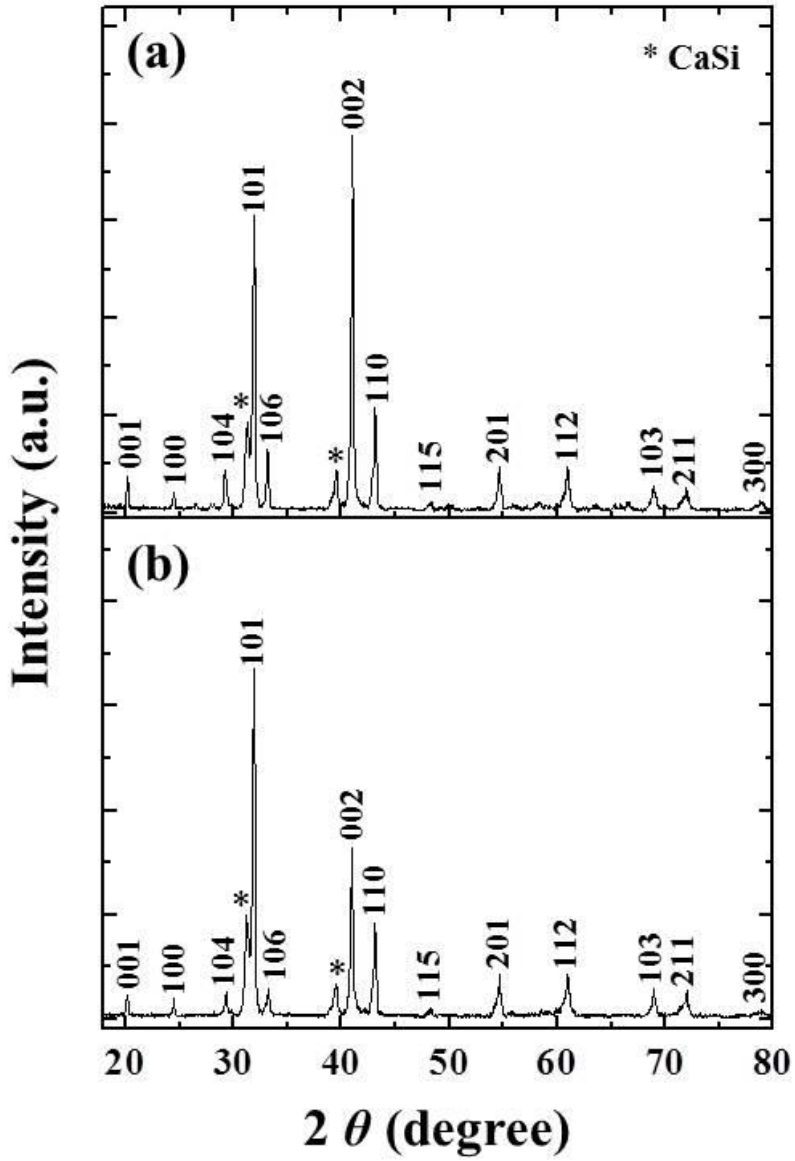

Fig. 1-1. XRD patterns of (a) $(Ca_{0.97}Eu_{0.03})AlSi$ and (b) $(Ca_{0.97}Eu_{0.03})AlSiH_x$ powders.

Table 1-1. Lattice parameters for $(Ca_{0.97}Eu_{0.03})AlSi$ and $(Ca_{0.97}Eu_{0.03})AlSiH_x$

Samples	Space group	*a* (Å)	*c* (Å)	*c*/*a*	Volume (Å^3)
(a) $(Ca_{0.97}Eu_{0.03})AlSi$	P6/mmm	4.220 (2)	4.422 (5)	1.047 (7)	68.212(3)
(b) $(Ca_{0.97}Eu_{0.03})AlSiH_x$		4.191 (2)	4.621 (2)	1.102 (5)	70.302(5)

Two kinds of the $CaAlSiN_3:Eu^{2+}$ phosphors were prepared from the (Ca,Eu)AlSi (as arc-melted) and (Ca,Eu)$AlSiH_x$ (as further hydrogenated) powders, respectively. Their XRD patterns are shown in Fig. 1-2. The reflection peaks of the $CaAlSiN_3:Eu^{2+}$ phosphor prepared

from the metal hydride powder were well assigned based on those of literatures [14, 16-18], but the another CaAlSi(O_xN_{3-x}):Eu^{2+} phosphor prepared from the (Ca,Eu)AlSi powder only gave the XRD pattern while was still mixed with several peaks originated from the impurity phase of AlN which usually depressed the emission intensity of $CaAlSiN_3$:Eu^{2+} phosphor.

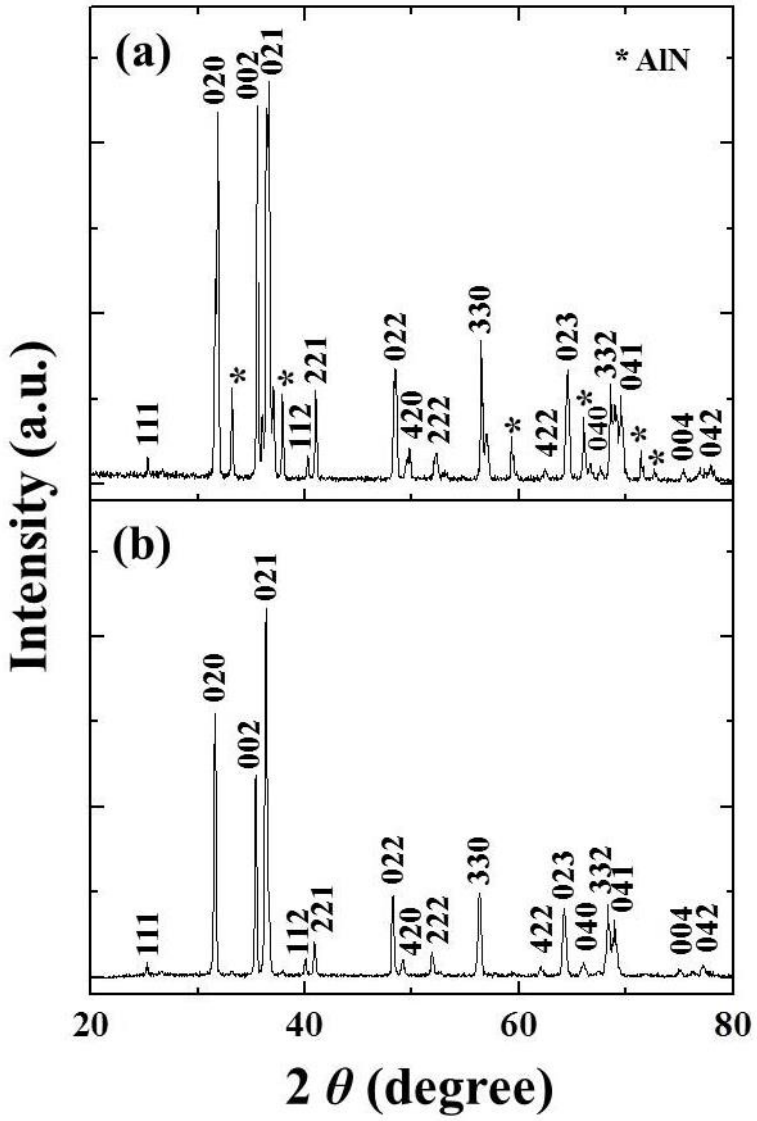

Fig. 1-2. XRD patterns of the $CaAlSiN_3$:Eu^{2+}(3 at%) phosphors prepared from (a) $(Ca_{0.97}Eu_{0.03})AlSi$ and (b) $(Ca_{0.97}Eu_{0.03})AlSiH_x$ powders.

The direct-nitriding processes using (Ca,Eu)AlSi and (Ca,Eu)$AlSiH_x$ powders are schematically illustrated in Fig. 1-3, together with the energy diagram for direct formation of Ca

→ Ca_3N_2 and indirect formation of Ca → CaH_2, respectively. For the direct-nitriding process using metal or alloy (intermetallic compound) powders, the raw materials usually sinter and/or melt together to form enlarged metal particles because most of nitriding processes for metals or alloys (intermetallic compounds) take place exothermically and the temperature of such raw materials extremely increases due that they release extra amounts of heat for producing the corresponding metal nitrides. Consequently, the effective surface area of such raw materials should be decreased with forming such sintered or melted metal particles with the enlarged particle sizes. As a result, the core parts of such particles hardly react with nitrogen, so that the nitriding reaction never takes place uniformly and the raw materials used remain as metallic residues. For the $CaAlSiN_3:Eu^{2+}$ phosphor, the samples prepared from the (Ca,Eu)AlSi powder were colored with dark-red without an exception and the emission intensity of them was usually low. Contrastively, by using the (Ca,Eu)$AlSiH_x$ powder, the nitriding reaction took place uniformly to produce the $CaAlSiN_3:Eu^{2+}$ phosphor bulks colored with clear red. This means that the reactivity of (Ca,Eu)$AlSiH_x$ powder with the mean particle size below 20 μm is much higher than that of the (Ca,Eu)AlSi powder.

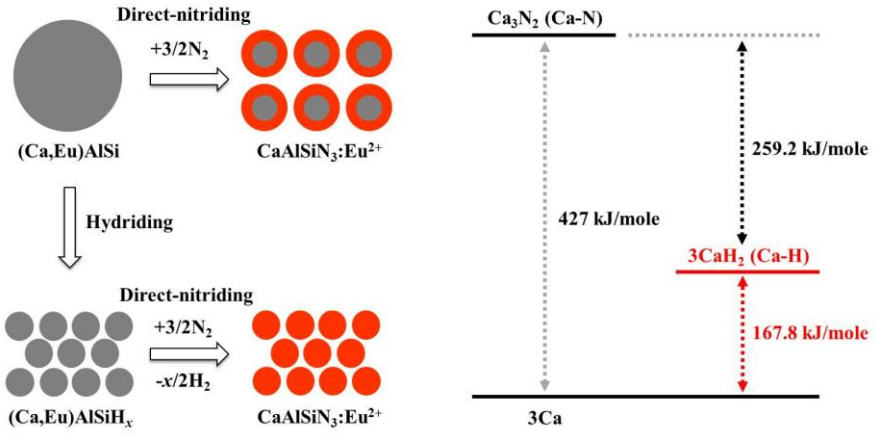

Fig. 1-3. Schematic illustration of the direct-nitriding processes using (Ca,Eu)AlSi and (Ca,Eu)$AlSiH_x$ powders (left side), together with the energy diagram for direct formation of Ca → Ca_3N_2 and indirect formation of Ca → CaH_2 → Ca_3N_2 (right side).

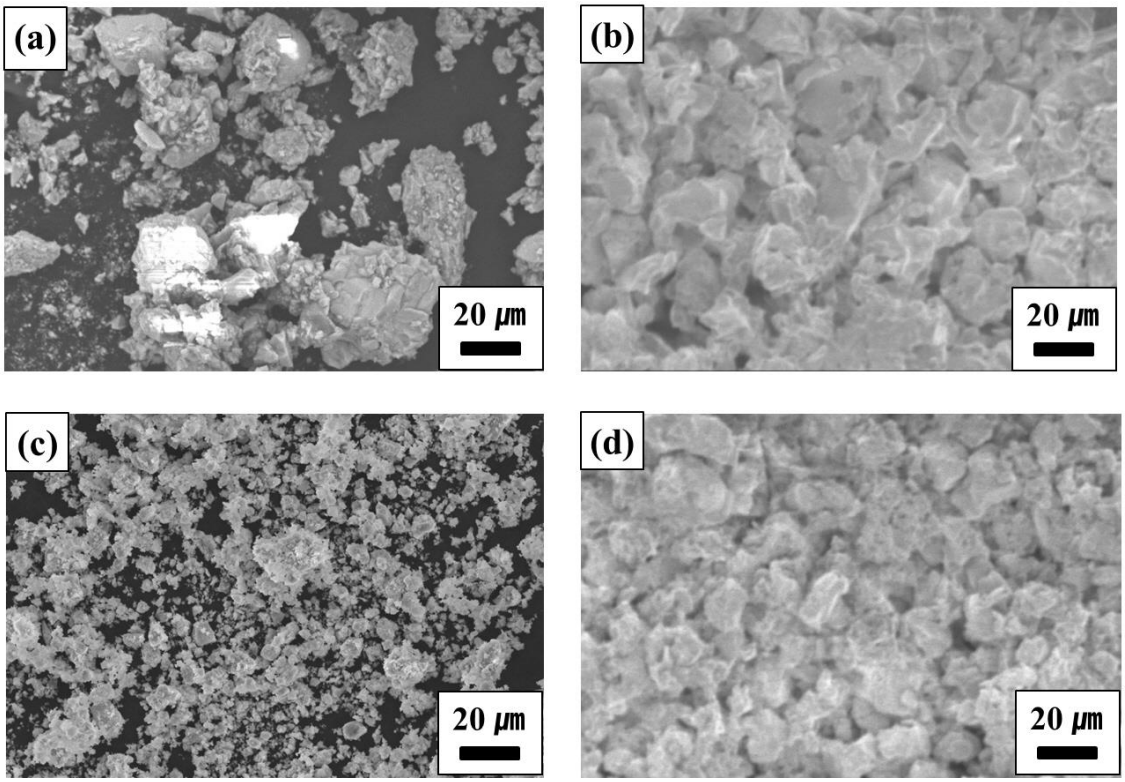

Fig. 1-4. SEM images for (a) $(Ca_{0.97}Eu_{0.03})AlSi$ and (b) the resultant $CaAlSiN_3:Eu^{2+}$(3 at%) phosphor, and (c) $(Ca_{0.97}Eu_{0.03})AlSiH_x$ and (d) the resultant $CaAlSiN_3:Eu^{2+}$(3 at%) phosphor, respectively.

The typical SEM images of samples are shown in Fig. 1-4. It is clear that the $CaAlSiN_3:Eu^{2+}$ phosphor (image d) prepared from the (Ca,Eu)$AlSiH_x$ powder (image c) is consisting of the fine particles with the smaller size than the phosphor sample (image b) prepared from the (Ca,Eu)AlSi powder (image a). From the SEM views (b) and (d), the particle size of the $CaAlSiN_3:Eu^{2+}$ powder (average: 16 μm) prepared from the (Ca,Eu)$AlSiH_x$ one is found to be smaller than that of another phosphor powder (average: 26 μm) prepared from the (Ca,Eu)AlSi powder. This is due to the (Ca,Eu)$AlSiH_x$ powder of which the mean particle size (view b) is much smaller compared with that of the (Ca,Eu)AlSi powder (view a). In addition, since any aggregation among such raw material particles hardly takes place for the (Ca,Eu)$AlSiH_x$ powder, the reactivity of such metal hydride powder with the primary particle size of ~1 μm should be higher than that of the (Ca,Eu)AlSi powder. As discussed above, furthermore, (Ca,Eu)$AlSiH_x$, has already released a part of total formation energy for the direct-nitriding reaction:

$(Ca,Eu)AlSi + 3/2N_2 \rightarrow CaAlSiN_3:Eu^{2+} + \Delta Q_1$,

$(Ca,Eu)AlSiH_x + 3/2N_2 \rightarrow CaAlSiN_3:Eu^{2+} + (x/2)H_2\uparrow + \Delta Q_2$,

where $\Delta Q_1 > \Delta Q_2$. Therefore, the fine powder of $(Ca,Eu)AlSiH_x$ is good raw material to produce the $CaAlSiN_3:Eu^{2+}$ phosphor even under much moderate conditions, atmospheric pressure and 1450-1500^oC, without any formation of enlarged metallic particles.

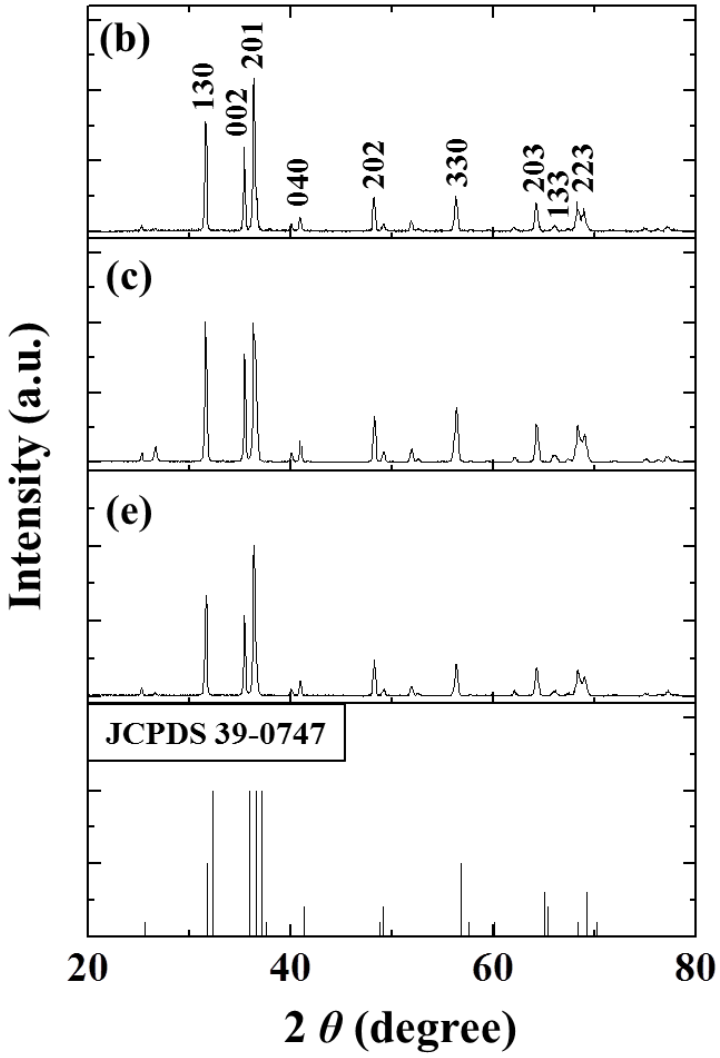

Fig. 1-5. XRD patterns of the $CaAlSiN_3:Eu^{2+}$(3 at%) phosphors prepared from the $(Ca_{0.97}Eu_{0.03})AlSiH_x$ powder mixed with (b) 0, (c) 10, and (e) 30 wt% of CaH_2 powder.

Fig. 1-5 shows the XRD patterns for the $CaAlSiN_3:Eu^{2+}$(3 at%) phosphors prepared from the $(Ca,Eu)AlSiH_x$ powders mixed with (b) 0, (c) 10, (e) 30 wt% of CaH_2 powder. All XRD patterns

are similar to the reflection profile reported elsewhere as a single phase [14, 16-18], meaning that all samples crystallize in an orthorhombic symmetry (*Cmc2₁*). The lattice parameters of sample e were refined to be a = 9.735(3), b = 5.647(2), and c = 5.048(7) Å. Also, the Rietveld refinement made for the XRD patterns measured on the sample e of which the chemical formular was estimated as $CaAlSiN_3:Eu^{2+}$(3 at%). The resultant atomic coordinates and thermal parameters are summarized in Table 1-2. In accordance with the space group of *Cmc2₁*, Al and Si atoms randomly distribute at the 8b site as well as Ca and Eu atom on the 4a one. In addition, any phase such as CaO or $Ca(OH)_2$ was not detected although an excess amount of Ca metal was charged to prepare the (Ca,Eu)AlSi intermetallic compound because the resultant $CaAlSiN_3:Eu^{2+}$ powders were immersed in the acidic solution to remove the impurities. Sintered bodies of the $CaAlSiN_3:Eu^{2+}$ phosphor took out from the RF furnace used for heating were colored with bright-orange homogeneously.

Table 1-2. Atomic coordinates and isotropic displacement parameters for the $CaAlSiN_3:Eu^{2+}$(3 at%) phosphor prepared from the $(Ca_{0.97}Eu_{0.03})AlSiN_3$ powder mixed with 30 wt% of CaH_2 powder

Atom	Site (*Cmc2₁*)	Coordinates[a)]			U_{iso} (Å^2)[a)]
		x	*y*	*z*	
Ca,Eu	4a	0	0.3147(5)	0.9749(5)	0.0165(2)
Al/Si	8b	0.1712(7)	0.8421(7)	0.0481(7)	0.0034(8)
N(1)	8b	0.2089(2)	0.8729(6)	0.4062(6)	0.0003(1)
N(2)	4a	0	0.2301(5)	0.5000(0)	0.0003(3)

[a)] R_p = 12.6 %, R_{wp} = 13.7 %, R_{exp} = 12.4 %.

The differential profile between the observed and calculated XRD patterns for the $CaAlSiN_3:Eu^{2+}$(3 at%) phosphor prepared from the $(Ca_{0.97}Eu_{0.03})AlSiH_x$ powder mixed with 30 wt% of CaH_2 powder is shown in Fig. 1-6. One can see that the observed pattern is in good accordance with the calculated one due that the differential profile between these is so flat. This means that the $CaAlSiN_3:Eu^{2+}$ powders prepared from the (Ca,Eu)$AlSiH_x$ powders scarcely contain any impurity such as AlN (see Figs. 1-2 (b) and 1-5).

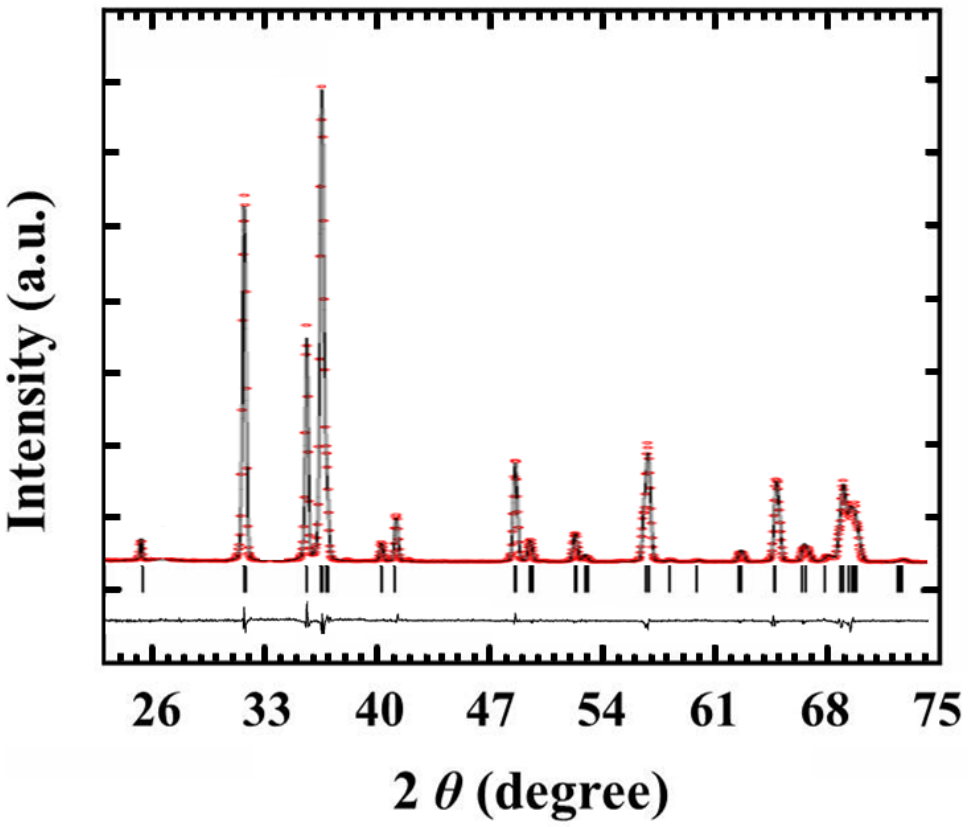

Fig. 1-6. Differential profile between the observed (circle) and calculated (line) XRD patterns for the $CaAlSiN_3:Eu^{2+}$(3 at%) phosphor prepared from the $(Ca_{0.97}Eu_{0.03})AlSiH_x$ powder mixed with 30 wt% of CaH_2 powder. The atomic coordinates and thermal parameters listed in Table 2 were used for the evaluation.

The SEM images for the $CaAlSiN_3:Eu^{2+}$(3 at%) phosphors prepared from the metal hydride powders mixed with (b) 0, (c) 10, and (e) 30 wt% of CaH_2 powder are shown in Fig. 1-7. For the $CaAlSiN_3:Eu^{2+}$ phosphor prepared only from the $(Ca,Eu)AlSiH_x$ powder (sample b), the cleavage planes of individual particles were not smooth and the other small particles adhered to their surface. However, with increasing the amount of CaH_2 powder as the flux (samples c and e), the surface of such cleavage planes became much smooth and, especially for the sample (e), the particles were facetted like single crystals and the mean size of these was evaluated to be about 20 μm.

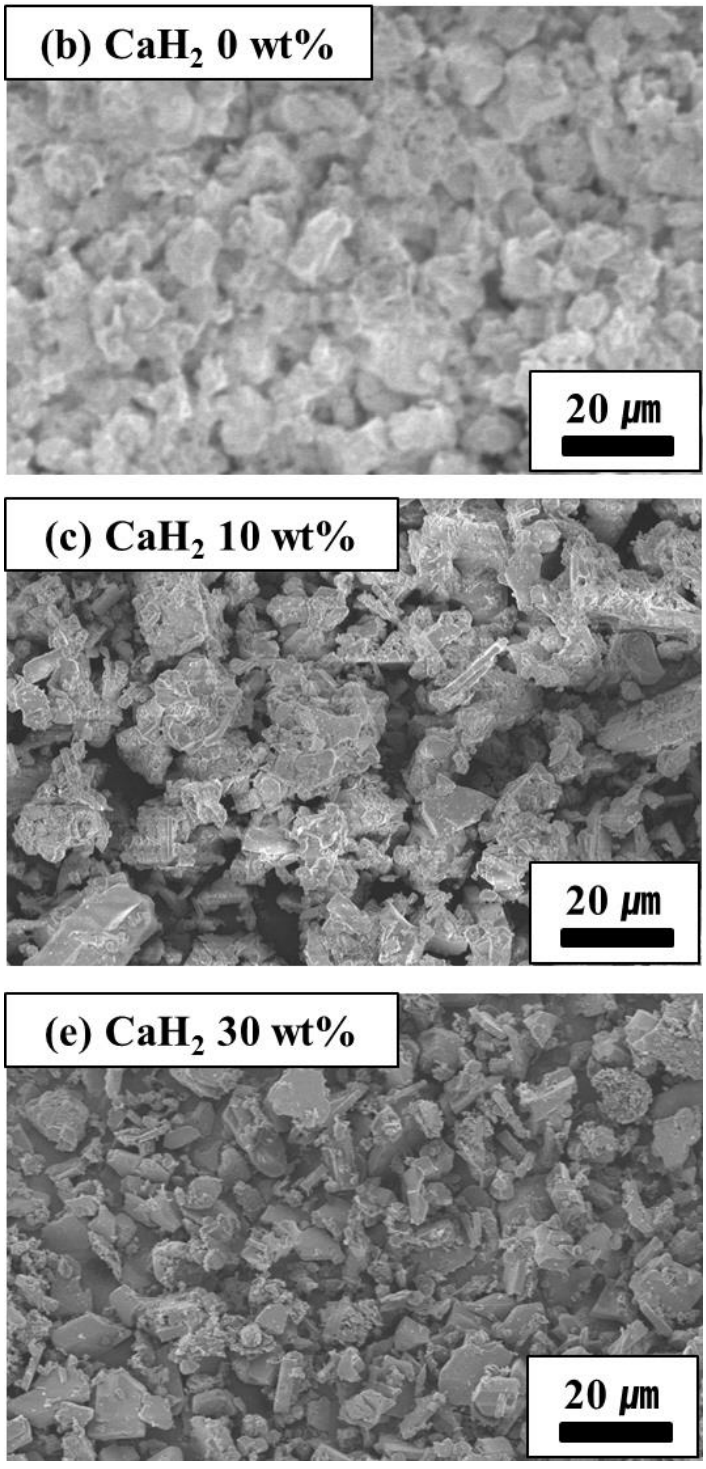

Fig. 1-7. SEM images of the $CaAlSiN_3:Eu^{2+}$(3 at%) phosphors shown in Fig 5.

Fig. 1-8 shows excitation and emission spectra for the $CaAlSiN_3:Eu^{2+}$ phosphors prepared from (a) as-obtained (Ca,Eu)AlSi and (b) hydrogenated (Ca,Eu)$AlSiH_x$ powders, respectively. Both the resultant phosphors gave the broad excitation bands covering from 300 to 600 nm which

were commonly peaking at about 450 nm. Consequently, under the excitation at these peak positions, red emissions were observed at 644 and 647 nm for the $CaAlSiN_3:Eu^{2+}$ phosphors prepared from the (Ca,Eu)AlSi and (Ca,Eu)$AlSiH_x$ powders, respectively, although the emission intensity of them was still weak: The relative intensity of sample b was about 66% of the intensity (100%) for YAG:Ce^{3+} (P46-Y3) standard phosphor. These emission bands are attributable to the allowed $4f^6 5d \rightarrow 4f^7$ transition of Eu^{2+} ion and the peak positions of excitation spectra around 450 nm fairly match well with the emission peak position of Ga(In)N-based blue LED chip (460 nm).

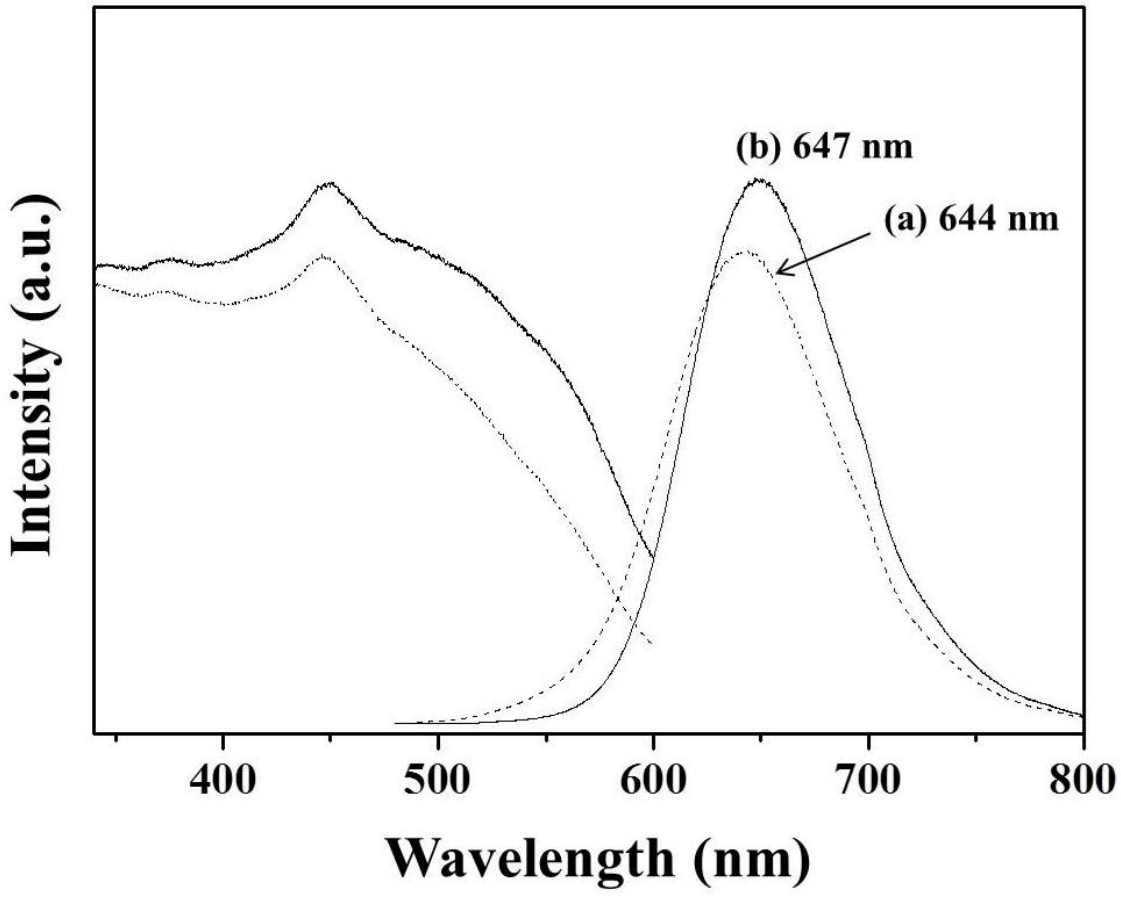

Fig. 1-8. Typical luminescence spectra of the $CaAlSiN_3:Eu^{2+}$(3 at%) phosphors prepared from (a) $(Ca_{0.97}Eu_{0.03})AlSi$ alloy and (b) $(Ca_{0.97}Eu_{0.03})AlSiH_x$ powders without mixing with CaH_2, respectively.

The emission peak position and intensity of $CaAlSiN_3:Eu^{2+}$ phosphors are strongly influenced by the content of oxygen impurity. The peak position is shifted to the shorter wavelength side and the intensity is lowered with increasing the content of such oxygen. Oxygen contents of the $CaAlSiN_3:Eu^{2+}$ phosphors prepared from the (Ca,Eu)AlSi and (Ca,Eu)$AlSiH_x$ powders were 4.21 and 3.07 wt% (see Table 1-3, samples a and b) that were extremely high compare with the value of the $CaAlSiN_3:Eu^{2+}$ phosphor synthesized by the CRN method using $CaCN_2$ as one raw material for reducing $CaCO_3$ to Ca_3N_2, $CaCN_2 + CaCO_3 \rightarrow 2/3\ Ca_3N_2 + CO_2 + CO + 1/2\ N_2$ [19]. However, it is noted that, for the $CaAlSiN_3:Eu^{2+}$ phosphor (sample b), the oxygen content is relatively low and thus, the emission intensity is higher than that of the sample (a).

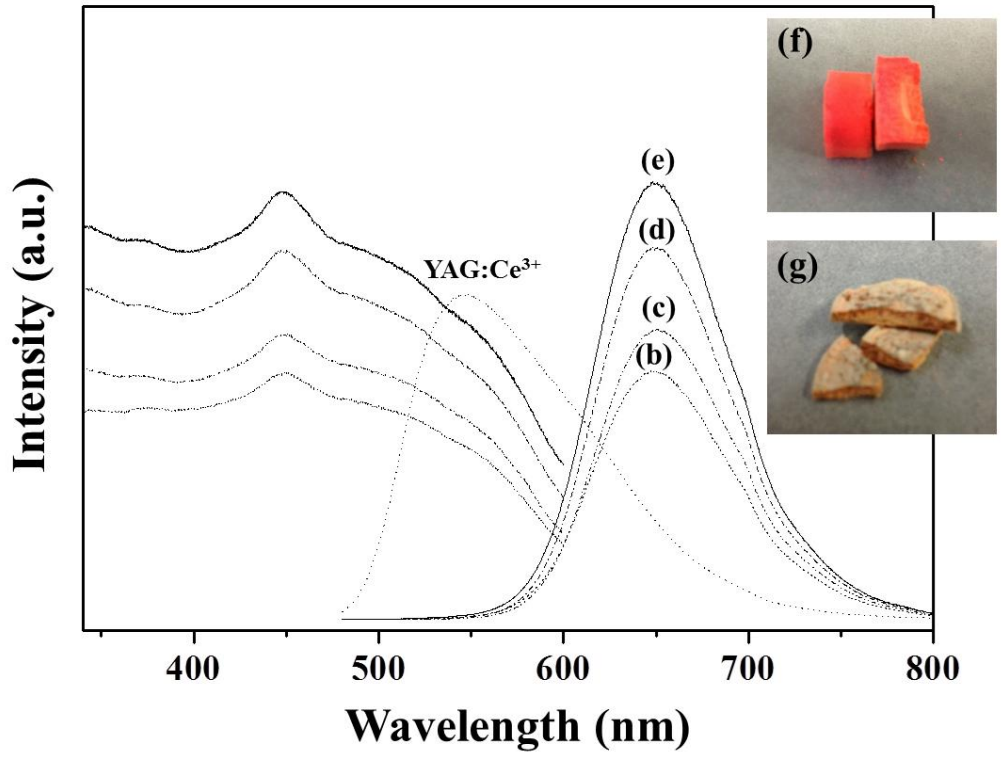

Fig. 1-9. Luminescence spectra of the $CaAlSiN_3:Eu^{2+}$(3 at%) phosphors prepared from $(Ca_{0.97}Eu_{0.03})AlSiH_x$ powders mixed with (b) 0, (c) 10, (d) 20, and (e) 30 wt% of CaH_2 powder, together with that of $YAG:Ce^{3+}$ (P46-Y3) phosphor as a reference. Inset photographs (f) and (g) at the right side correspond to the samples (e) and (b), respectively.

In order to reduce the content of oxygen impurity, various amounts of CaH_2 powder were added to the (Ca,Eu)$AlSiH_x$ powder. The concentration dependences of CaH_2 powder on the luminescence properties of $CaAlSiN_3:Eu^{2+}$(3 at%) phosphor are shown in Fig. 1-9. It is obvious that the emission intensity is much higher than that of the $CaAlSiN_3:Eu^{2+}$ phosphor prepared without any addition of CaH_2 powder. When the amount of CaH_2 powder was increased, the emission intensity gradually increased and finally approached to 110% of that for $YAG:Ce^{3+}$ (P46-Y3) standard phosphor. Also, photographs of the resultant $CaAlSiN_3:Eu^{2+}$ phosphor bulks (samples b and e) are shown in Figs. 1-9 (f) and (g). From Fig 1-9 (f), one can see that phosphor bulk is uniformly colored with clear orange and that the nitriding reaction proceeds even in the core parts. In the Table 1-3, the luminescence properties of the $CaAlSiN_3:Eu^{2+}$ are summarized together with their O/N contents.

Table 1-3. Luminescence properties and O/N contents for the $CaAlSiN_3:Eu^{2+}$(3 at%) phosphors prepared from the $(Ca_{0.97}Eu_{0.03})AlSi$ or $(Ca_{0.97}Eu_{0.03})AlSiH_x$ powders mixed with various amounts of CaH_2 powder

Samples	Raw composition	λ_{em} (nm)	λ_{ex} (nm)	RI (%)[a)]	O (wt%)	N (wt%)
(a)	$(Ca_{0.97}Eu_{0.03})Al_{0.9}Si$	450	644	63	4.21	20.41
(b)	$(Ca_{0.97}Eu_{0.03})Al_{0.9}SiH_x$	450	647	66	3.07	21.97
(c)	$(Ca_{0.97}Eu_{0.03})Al_{0.9}SiH_x$ + CaH_2 (10 wt%)	450	650	76	2.29	23.34
(d)	$(Ca_{0.97}Eu_{0.03})Al_{0.9}SiH_x$ + CaH_2 (20 wt%)	450	650	94	1.34	24.06
(e)	$(Ca_{0.97}Eu_{0.03})Al_{0.9}SiH_x$ + CaH_2 (30 wt%)	450	650	110	0.72	28.74
(f)	$(Ca_{0.97}Eu_{0.03})Al_{0.9}SiH_x$ + CaH_2 (40 wt%)	450	650	97	0.80	29.02
(g)	$YAG:Ce^{3+}$ (P46-Y3)	460	544	100	-	-

[a)] Relative emission intensity.

Typical temperature dependence curves of the emission intensity for the $CaAlSiN_3:Eu^{2+}$(3 at%) phosphors prepared from (a) the (Ca,Eu)AlSi powder and (b) the (Ca,Eu)$AlSiH_x$ powder mixed with 30 wt% of CaH_2 one are shown in Fig. 1-10, together with that of the $YAG:Ce^{3+}$ standard phosphor. At 150°C, the degradation of intensity was only 6~17% of the initial value at room temperature for the $CaAlSiN_3:Eu^{2+}$(3 at%) phosphors but 33 % for the $YAG:Ce^{3+}$ (PY46-Y3) phosphor. Especially, the $CaAlSiN_3:Eu^{2+}$(3 at%) phosphor prepared from the hydride powder can keep much high emission intensity at high temperature compared with the another

phosphor prepared from the (Ca,Eu)AlSi powder.

Although the origin of excellent thermal stability of nitride phosphors has not been well clear, this is responsible for three-dimensional network of the $(Si,Al)N_4$ tetrahedra which consist of strong Si-N and Al-N covalent bonds. This kind of rigid structural framework lowers the vibrational energy state from the emission center level and thus, the energy loss caused by the nonradiative transition from the excited state to the ground one is suppressed even under the high temperature condition [8]. The small thermal quenching property of $CaAlSiN_3:Eu^{2+}$ phosphor is desirable for using them as the solid illumination parts which are usually working at about 150°C.

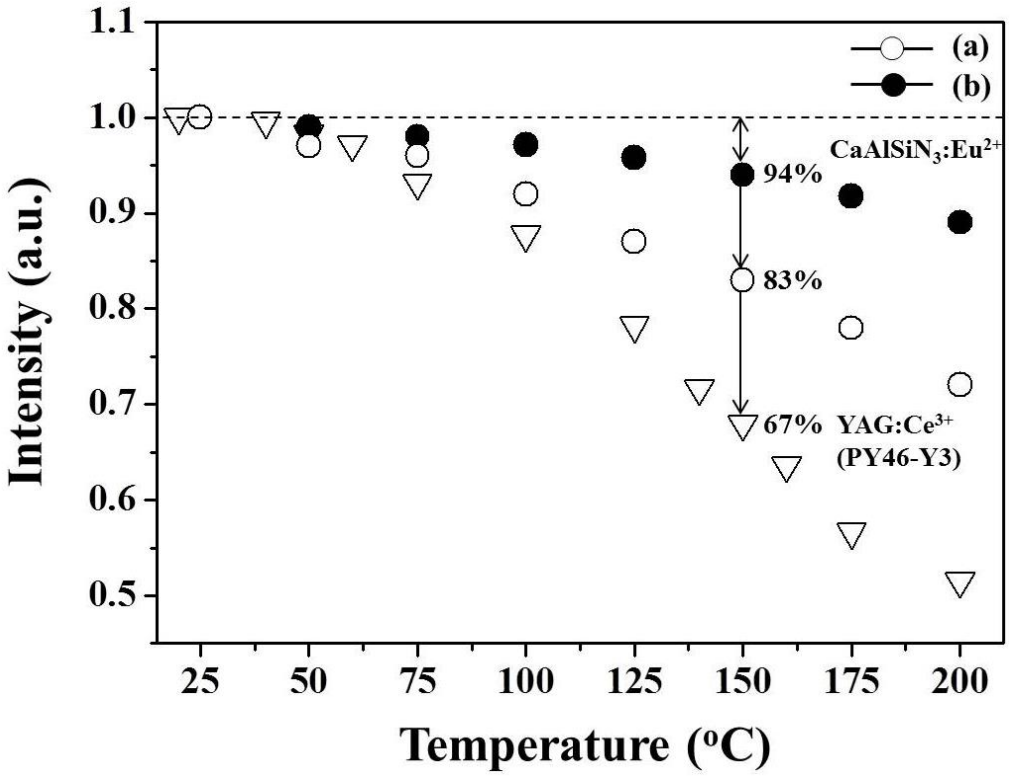

Fig. 1-10. Temperature dependences for the emission intensity of $CaAlSiN_3:Eu^{2+}$(3 at%) phosphors prepared from the (a) $(Ca_{0.97}Eu_{0.03})AlSi$ and the (b) $(Ca_{0.97}Eu_{0.03})AlSiH_x$ powder mixed with 30 wt% of CaH_2 together with that of the $YAG:Ce^{3+}$ (P46-Y3) phosphor as the reference.

1.2 (Sr,Ca)$AlSiN_3$:Eu^{2+} phosphor

1.2.1 Introduction

In 2008, Watanabe and co-workers [20] have reported that $SrAlSiN_3$:Eu^{2+} is one of much notable phosphors to provide the emission band peaking at 610 nm which is much close to the red isochromatic region around 615 nm compared with $CaAlSiN_3$:Eu^{2+} (about 655 nm). However, Sr atom is a little too large to share 4a site ($Cmc2_1$) in a three-dimensional $(Al_2Si_2N_{12})_n$ network consisting of AlN_4 and SiN_4 tetrahedral units, so that any host lattice of $SrAlSiN_3$ has not been synthesized even by the direct nitriding method using low alloy powders under mild-pressure conditions of N_2 gas below 1 MPa up to date [20,21]. Also, the other synthesis route using the $Sr_2N_{0.92}$ powder as a Sr source, which is of strong deliquescence and high cost, is at least required the same high-pressure condition as 190 MPa and the production yield is much low (ca 1 %) [22]. Only by replacing Ca atom with Sr one, (Sr,Ca)$AlSiN_3$:Eu^{2+} phosphors have been reported to produce from the corresponding (Sr,Ca)AlSi alloy precursors in each single phase form under the high-pressure condition of N_2 gas on a hot isostatic pressing apparatus [9,22-24], because the sublimation of Sr metal extremely takes place at the temperature around the boiling point (bp = 1382 ^oC) before such direct nitriding process for metals. Furthermore, several groups have been succeeded in synthesizing such metal nitride phosphors by applying unique techniques, *e.g.* ammothermal synthesis [24], spark plasma firing [25], and metathesis reactions [26] at low temperature. However, most of these methods also required high-pressure conditions of 0.9 to 190 MPa.

Meanwhile, new direct nitriding method using metal hydrides precursors as the raw materials, Si/MSi_2H_x (M = Ca, Sr, Ba), has been proposed to produce the corresponding $M_2Si_5N_8$:Eu^{2+} phosphors with good luminescence properties [14], because most of metals and alloys are easily pulverized by a hydrogen absorbing effect so called “hydrogen embrittlement”.

In this work, the (Sr,Ca)$AlSiN_3$:Eu^{2+} phosphors were synthesized from the mixtures of (Sr,Eu)$AlSiH_x$ powders derived from (Sr,Eu)AlSi alloys and CaH_2 powder added as a flux under atmospheric-pressure (*ca*. 0.1 MPa) heating conditions, where these metal hydrides were highly reactive to N_2 gas and the excess amounts of alkaline earth elements were serve to grow up the crystalline particles of phosphors free from any impurity phase. The resultant phosphors were

characterized to meet the requirements of the red light source for LED solid illumination.

1.2.2 Experimental Section

Metal hydride powders were obtained from the $Sr_{1.1}Eu_{0.02}AlSi$ or $Ca_{1.1}Eu_{0.02}AlSi$ alloy, which was prepared by arc melting of Sr (99.0 %) or Ca (99.0 %), Eu (99.5 %), Al (99.99 %), and Si (99.9999 %) metals in a Ar gas (99.999 %), under a high-pressure heating condition, 3.0 MPa of H_2 gas, 450 ^{o}C for 1 h. Since the boiling point of Sr or Ca metal was low (Sr, 1382 °C; Ca, 1484 °C), 10 at% excess amount of these metals were used for the preparation of two alloy ingots. Several portions of resultant metal hydride powders were intimately mixed with various amounts of CaH_2 powder, individually, and then each of them was charged in a BN crucible, followed by loading into a radio frequency (RF) furnace equipped with a ZrB_2 heater. The reaction chamber was fulfilled with a highly purified N_2 gas (99.9999 %) after evacuating and then heated under a flow condition of N_2 gas (20 ml/min). The temperature was slowly increased at a rate of 10 °C/min up to 1050 °C and kept for 2 h, because the ignition for nitrogenizing the raw materials took place at about 1060 °C that the alloy particles were sintered together and the cores of them were hardly nitrogenized. Finally, the heating temperature was rapidly increased and kept at 1450–1550 °C for 6 h. The fired samples were cooled to room temperature in the furnace and, after roughly grinding, the phosphor powders were washed with a 1 N HCl solution to remove the excess amount of Sr or Ca metal, the Ca_3N_2 residue derived from CaH_2, and so on.

XRD patterns of resultant phosphors were measured on an X-ray powder diffractometer (RINT2200, Rigaku) using a monochromated Cu Kα radiation to identify the M'$AlSiN_3$ host lattice phases. Photoluminescence (PL) spectra were recorded on a fluorescence spectrophotometer (F-4500, Hitachi) at room temperature. Also, the temperature dependence curves of emission intensity were measured for them by monitoring the corresponding peak heights of emission bands on a photomultiplier (USB2000, Oceans Optics) in a range of RT and 200 ^{o}C. The relative intensity of resultant phosphors was evaluated by referring a commercially available YAG:Ce^{3+} phosphor (P46-Y3, KASEI Optonix). The particle morphology of phosphors were observed by field emission scanning electron microscopy (FE-SEM; ERA-8800, ELIONIX) equipped with an energy dispersive X-ray (EDX) spectroscopy unit.

1.2.3 Result and Discussion

Fig. 1-11 shows XRD patterns of (Sr,Ca)$AlSiN_3$:Eu^{2+} phosphors produced from the $Sr_{1.1}Eu_{0.02}AlSiH_x$ powder by mixing with various amounts of CaH_2 ((a) - (e) : 0 - 30 wt%), together with that for the $Ca_{1.1}Eu_{0.02}AlSiH_x$ powder (f) as heated at 850 ^oC for 2 h and 1500 ^oC for 6 h without adding CaH_2. The peaks observed on the samples (a) and (b) suggested that the resultant materials contained $Sr_2Si_5N_8$:Eu^{2+} (or $(Sr,Ca)_2Si_5N_8$) and AlN as impurity phases, other than the purpose material of $SrAlSiN_3$ (or (Sr,Ca)$AlSiN_3$). A series of peaks on the XRD pattern of sample (a) were assigned to $SrAlSiN_3$ phase although the intensity of them was weak. This result allows us to conclude that the hydrogenated alloy powder, $Sr_{1.1}Eu_{0.02}AlSiH_x$, forms the $SrAlSiN_3$ crystal lattice even under this ambient pressure heating condition. The sample (c) also accompanied the $(Sr,Ca)_2Si_5N_8$ phase, but the main phase was the purpose material of (Sr,Ca)$AlSiN_3$.

For the XRD patterns of samples (d), (e), and (f), most of the peaks were assigned according to the cell data of $CaAlSiN_3$ (JCPDS card: 39-0747, orthorhombic, *Cmc*2_1) although a few unknown, weak peaks (around $2\theta = 26^o$, 51^o, 61^o) were still detected even on the samples (d) and (e). It means that the (Sr,Ca)$AlSiN_3$:Eu^{2+} phosphors were obtained as the almost single phase with the same crystallographic symmetry as that of $CaAlSiN_3$.

Inset Fig.1-11 (a) and (d) show photographs of the corresponding samples which have been produced from $Sr_{1.1}Eu_{0.02}AlSiH_x$ without or with 20 wt% of CaH_2 as the flux, respectively, which are corresponding to the XRD patterns (a) and (d). Whereas the sample (a) was colored with dark green and the emission intensity was considerably low as described later, the sintered body of sample (d) was uniformly colored with bright red. This means that the reactivity of metal hydride ($Sr_{1.1}Eu_{0.02}AlSiH_x$) is much higher than that of the as-obtained alloy, *viz*. $Sr_{1.1}Eu_{0.02}AlSi$, so that the purpose material of (Sr,Ca)$AlSiN_3$:Eu^{2+} is obtained as the high-quality form.

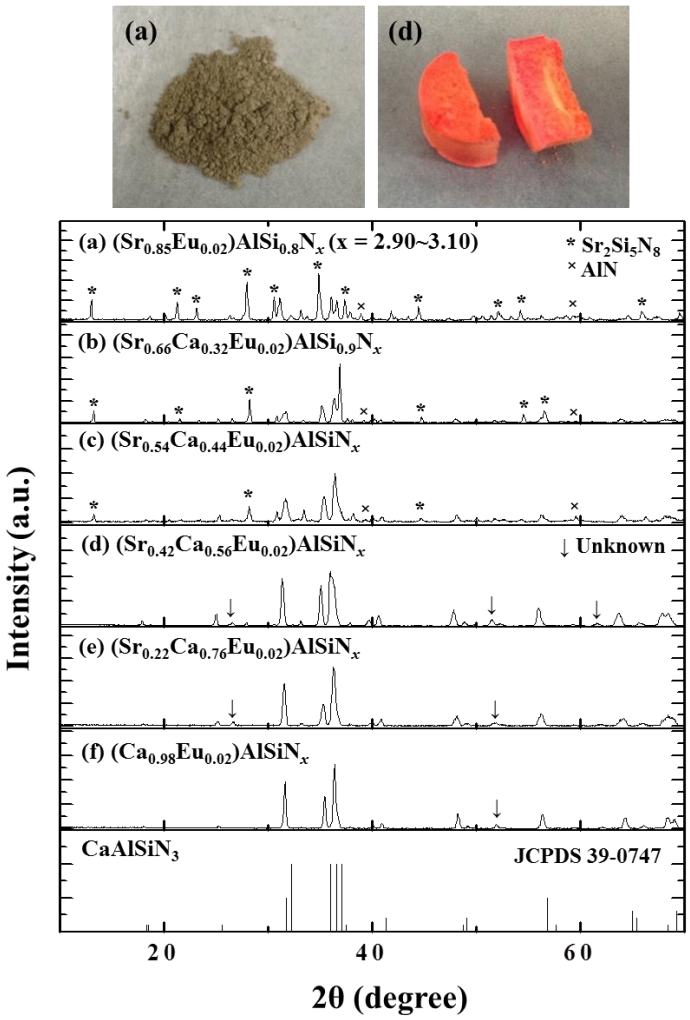

Fig. 1-11. XRD patterns of (Sr,Ca)$AlSiN_3$:Eu^{2+} phosphors prepared from the $Sr_{1.1}Eu_{0.02}AlSiH_x$ powder by adding various amounts of CaH_2: (a) 0, (b) 10, (c) 15, (d) 20, (e) 30 wt%, together that for the $Ca_{1.1}Eu_{0.02}AlSiH_x$ powder without CaH_2: (f). Inset photographs (a) and (d) are for the samples (a) and (d). The chemical compositions were analytical ones.

This was supported by the nitiriding characteristics of the as-obtained alloy ($Sr_{1.1}Eu_{0.02}AlSi$) and hydride ($Sr_{1.1}Eu_{0.02}AlSiH_x$) powders. The weight gain values (Δ w) and resultant phases for these raw materials as heated at 750-950 ^oC for 2 h in a N_2 gas flow are summarized in Table 1-4. The reactivity of $Sr_{1.1}Eu_{0.02}AlSi$ and $Sr_{1.1}Eu_{0.02}AlSiH_x$ was fairly evaluated by measuring the weight gain of both powders at 750, 850, and 950 ^oC on the conventional electric furnace used for producing the phosphorous materials. The alloy or hydride powder (250 mg) was charged in a Mo crucible and, after heating it under each condition, the resultant sample was weighted again and the XRD pattern was also measured to identify the formed phases under the heating

conditions. From Table 1-4, the weight of $Sr_{1.1}Eu_{0.02}AlSiH_x$ powder was clearly found to increase at 850 ^oC that was corresponding to $Sr_{1.1}Eu_{0.02}AlSiN_\alpha$ ($\alpha \leq 3$). This means that the reactivity of metal hydride ($Sr_{1.1}Eu_{0.02}AlSiH_x$) is much higher than that of the as-obtained alloy ($Sr_{1.1}Eu_{0.02}AlSi$). Therefore, one can understand that the reaction of metal hydride powders with N_2 effectively takes place before the sublimation of Sr metal even under the atmospheric-pressure heating conditions. However, CaH_2 is needed to form the well-crystallized host lattices of $M'AlSiN_3$.

Table 1-4. Weight gain values (Δw) and resultant phases of the alloy and hydride powders heated at 750-950 ^oC for 2 h in a N_2 gas flow

	$Sr_{1.1}Eu_{0.02}AlSi$			$Sr_{1.1}Eu_{0.02}AlSiH_x$		
Temperature (^oC)	750	850	950	750	850	950
Δ w (%)[a]	0.007	0.01	0.021	0.008	0.015	0.026
Phase[b]	A	N, A	N, A	A	N, A	N, A

[a]Mass %.

[b]A: alloy phase (SrAlSi), N: nitride phase (Sr/CaAlSiN$_3$ and AlN).

Luminescence spectra of $(Sr_{0.54}Ca_{0.44})AlSiN_x:Eu^{2+}$, $(Sr_{0.42}Ca_{0.56})AlSiN_x:Eu^{2+}$, and $(Sr_{0.22}Ca_{0.76})AlSiN_x:Eu^{2+}$ phosphors are shown in Fig. 1-12, together with that of a commercially-available YAG:Ce^{3+} (P46-Y3) phosphor. Under an excitation of 450 nm, all the phosphors gave strong and wide emission bands peaking at 635 - 655 nm (red region) and ranging from 500 to 800 nm. The excitation by 450 nm is generally ascribed to the parity-allowed transition $4f^7 \rightarrow 4f^6 5d^1$ of Eu^{2+} ion. The relative emission intensity of $(Sr_{0.42}Ca_{0.56})AlSiN_x:Eu^{2+}$ phosphor was about 90% of that of YAG:Ce^{3+} and the excitation spectrum was maximized at the wavelength around 450 nm which matched well with the emission peak position of InGaN-based blue LED chip (460 nm), suggesting that this phosphor was practically noted as the red color component for white LED solid illumination which creates "warm" white lights.

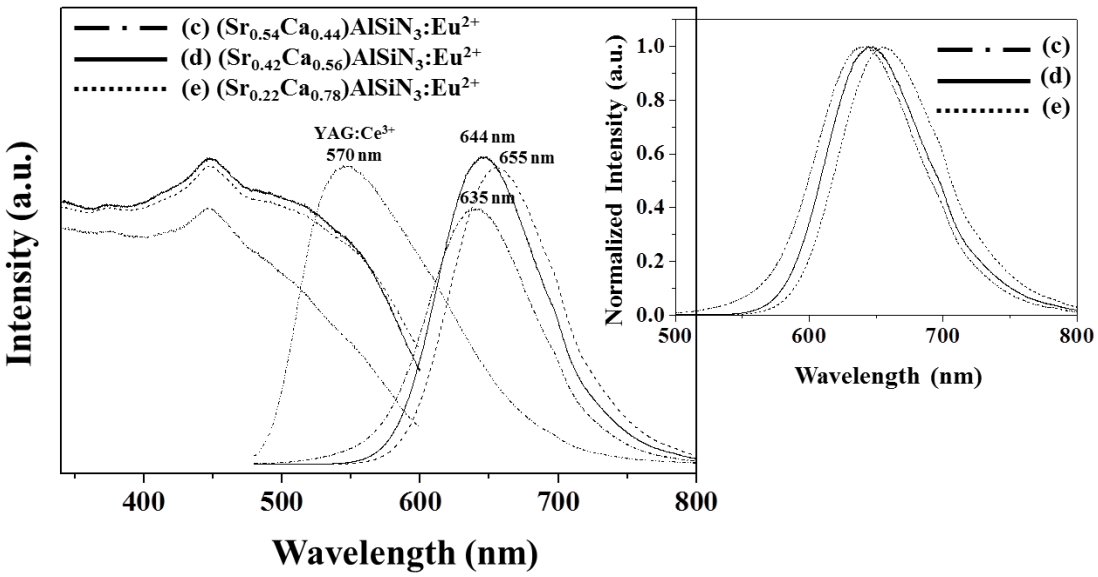

Fig. 1-12. Luminescence spectra of (Sr,Ca)$AlSiN_3$:Eu^{2+} phosphors, together with that of YAG:Ce^{3+} one as a reference.

Table 1-5. Analytical compositions, cell parameters, and luminescence properties of (Sr,Ca)$AlSiN_3$:Eu^{2+} phosphors

[a]Component (N_x[b]) Added CaH_2 (wt%)	Cell parameters				Luminescence properties		
	a (Å)	b (Å)	c (Å)	V (Å^3)	λ_{ex} (nm)	λ_{em} (nm)	*I* (%)
(a) $(Sr_{0.85}Eu_{0.02})AlSi_{0.8}N_x$ -[c]	9.84(6)	5.76(7)	5.17(5)	293.84	450	632	12
(b) $(Sr_{0.66}Ca_{0.32}Eu_{0.02})AlSi_{0.9}N_x$ 10[c]	9.82(1)	5.71(1)	5.11(4)	286.52	450	655	77
(c) $(Sr_{0.54}Ca_{0.44}Eu_{0.02})AlSiN_x$ 15[c]	9.82(1)	5.69(5)	5.11(1)	285.52	450	635	78
(d) $(Sr_{0.42}Ca_{0.56}Eu_{0.02})AlSiN_x$ 20[d]	9.82(3)	5.68(1)	5.09(6)	283.90	450	644	90
(e) $(Sr_{0.22}Ca_{0.76}Eu_{0.02})AlSiN_x$ 30[d]	9.81(7)	5.67(5)	5.08(8)	282.56	450	655	88
(f) $(Ca_{0.98}Eu_{0.02})AlSiN_x$ -[d, e]	9.81(2)	5.63(1)	5.06(7)	279.46	450	655	97

[a]Samples were prepared from $Sr_{1.1}Eu_{0.02}AlSiH_x$ and $Ca_{1.1}Eu_{0.02}AlSiH_x$, powders free from or with CaH_2 one (0-30 wt%) as a flux. [b]The nitrogen content values were analyzed to x = 2.90 ~ 3.10. [c]Samples were mixed with impurity phases. [d]Each sample was of a single phase. [e]Sample was prepared from $Ca_{1.1}Eu_{0.02}AlSiH_x$ powder free from CaH_2 one as a flux.

The compositional formulae of phosphors evaluated from the EDX data for samples (a) - (f) are summarized in Table 1-5, together with the cell parameters and luminescence data. For the

sample (a) prepared from $Sr_{1.1}Eu_{0.02}AlSiH_x$ without any use of CaH_2 as the flux, several peaks of the XRD pattern (see Fig. 1-11) suggested that the $SrAlSiN_3$ phase was formed even under the atmospheric-pressure heating condition to give the crystal lattice with cell parameters, *viz*. a = 9.84(6), b = 5.76(7), and c = 5.17(5) Å, although the production yield was very low. From the compositional values of samples (b) - (e), one can see that CaH_2 is served not only as the flux but also as the Ca source to produce the well-crystallized powders of $(Sr,Ca)AlSiN_3:Eu^{2+}$. The amount of Ca atom which was incorporated to the $SrAlSiN_3$ crystal lattice was gradually increased with increasing the charged amount of CaH_2. For the sample (a), the analytical values of composition (Sr + Eu = 0.87) was less than 1.00, due to the sublimation of Sr metal during the heat treatment at 1500 ^oC. This resulted in the formation of $Sr_2Si_5N_8$ phase as a main phase. However, the CaH_2 powder added as the flux compensates such loss of Sr metal, so that one can eventually produce the $(Sr,Ca)AlSiN_3:Eu^{2+}$ phosphors even under the atmospheric-pressure heating conditions, in which the Ca element is incorporated to the $SrAlSiN_3$ crystal lattice.

Whereas the sample (a) gave an emission band peaking at 632 nm, the peak positions observed on other samples were distributed in the longer wavelength range, 644 – 655 nm. The former result means that the emission band is mainly attributed to the $Sr_2Si_5N_8:Eu^{2+}$ phase since it is detected on the XRD pattern as the main phase and usually gives an intense red emission band at about 620 nm.

The emission band of sample (b) had the peak at 655 nm which was similar to that of sample (e) or (f). However, the sample (b) consisted of a mixture of $(Sr,Ca)_2Si_5N_8:Eu^{2+}$, AlN, and $(Sr,Ca)AlSiN_3:Eu^{2+}$ materials and thus, the analytical value of composition, $(Sr_{0.66}Ca_{0.32})AlSi_{0.9}N_x:Eu^{2+}$, was meaning-less and among these component materials, the main phase was the $(Sr,Ca)_2Si_5N_8:Eu^{2+}$ one. Since the Sr-rich $(Sr,Ca)_2Si_5N_8:Eu^{2+}$ phosphor gives a band emission peaking at the longer wavelength side (~ 640 nm) than those of $Sr_2Si_5N_3:Eu^{2+}$ (ca 620 nm) and $Ca_2Si_5N_3:Eu^{2+}$ (ca 600 nm) with the same dopant amount of Eu^{2+} (2 at%) [27]. Therefore, the peak position observed (655 nm) is mainly responsible for such Sr-rich $(Sr,Ca)_2Si_5N_8:Eu^{2+}$ phosphor .

The sample (c), $(Sr_{0.54}Ca_{0.44})AlSiN_x:Eu^{2+}$ also consisted of the similar mixture of $(Sr,Ca)AlSiN_3:Eu^{2+}$, $(Sr,Ca)_2Si_5N_8:Eu^{2+}$, and AlN phases as the sample (b), but the major phase was the $(Sr,Ca)AlSiN_3:Eu^{2+}$ one. Since the Sr-rich $(Sr,Ca)AlSiN_3:Eu^{2+}$ and Ca-rich $(Sr,Ca)_2Si_5N_8:Eu^{2+}$ phosphors gave red (620 - 650 nm) and orange (peak position = 600 - 620 nm)

emissions, respectively. The emission band peaking at 635 nm may be due to a combination effect of these two phosphors.

Contrary to the above results, the samples (d) and (e), $(Sr_{0.42}Ca_{0.56})AlSiN_x:Eu^{2+}$ and $(Sr_{0.22}Ca_{0.76})AlSiN_x: Eu^{2+}$ were produced in single phase forms with the orthorhombic symmetry and, among these, the peak position of $(Sr_{0.54}Ca_{0.44})AlSiN_x:Eu^{2+}$ phosphor (644 nm) was fairly shifted at the side close to the red isochromatic region around 615 nm. The relative intensity was ca 90% of that of YAG:Ce^{3+} (P46-Y3) phosphor, but the brightness of this phosphor should be improved by optimizing the preparation condition.

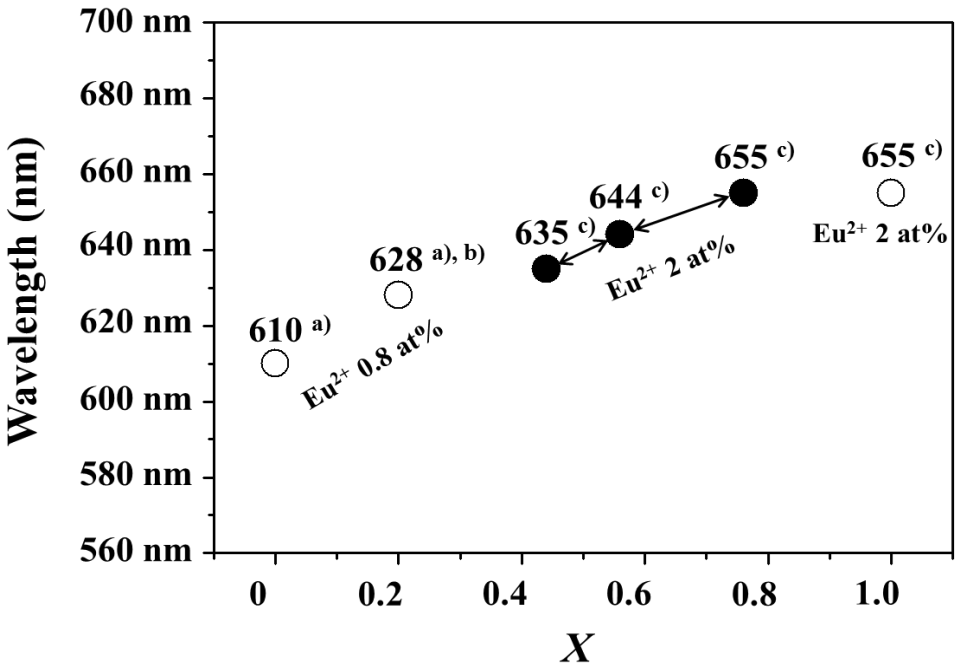

Fig. 1-13. A relationship between the emission peak position (wavelength) and Ca content (*x*) for $Sr_{1-x}Ca_xAlSiN_3:Eu^{2+}$ phosphors. [a]Ref. 11, [b]Ref. 6, [c]This work.

The emission peak wavelength values are plotted against each Ca content (*x*) for $Sr_{1-x}Ca_xAlSiN_3:Eu^{2+}$ phosphors (see Fig. 1-13). There was a clear correlation between those values that the emission band was shifted to the longer wavelength side with increasing the *x* value. This indicates that the blue shift of emission bands is attributable to the decrease in crystal field strength due that the cell size is expanded with increasing the Sr content in the host lattice. In this work, the concentration of Eu^{2+} ion as an activator (2 at%) was larger than that (0.8 at%)

for the (Sr,Ca)$AlSiN_3$:Eu^{2+} and $CaAlSiN_3$:Eu^{2+} phosphors reported elsewhere [8,23]. It is noteworthy that the emission band of (Sr,Ca)$AlSiN_3$:Eu^{2+} phosphor shifts to the red isochromatic region around 615 nm with increasing the Sr content in (Sr,Ca)$AlSiN_3$ host lattice [9,20].

Fig. 1-14 shows temperature dependence curves for the integrated emission intensity of ($Sr_{0.42}Ca_{0.56}$)$AlSiN_3$:Eu^{2+}(2 at%) phosphor, together with that of YAG:Ce^{3+} (P46-Y3) phosphor. At the working temperature of white LED lamps (150 ^oC), the emission intensity of ($Sr_{0.42}Ca_{0.56}$)$AlSiN_3$:Eu^{2+}(2 at%) phosphor excited at 450 nm was still maintained to be about 86% against that of room temperature, but that of YAG:Ce^{3+} phosphor was decrease to 68 %, in a similar manner as $CaAlSiN_3$:Eu^{2+} [19].

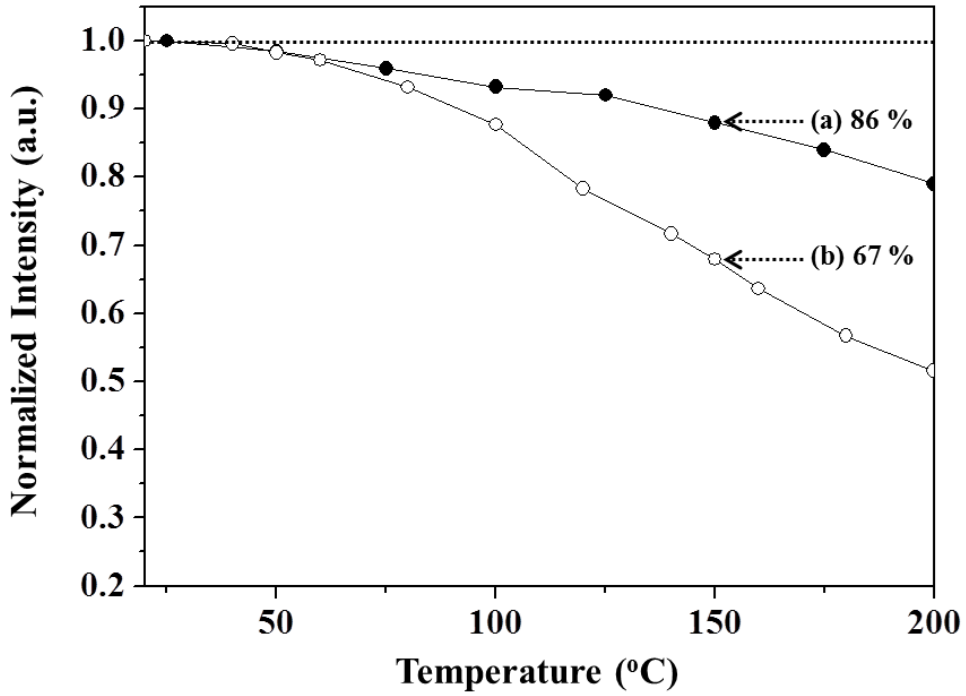

Fig. 1-14. Temperature dependence curves of emission peak intensity for (a) ($Sr_{0.42}Ca_{0.56}$)$AlSiN_3$:Eu^{2+}(2 at%) and (b) YAG:Ce^{3+} phosphors.

1.3 Conclusions

High-quality of $CaAlSiN_3$:Eu^{2+} and (Sr,Ca)$AlSiN_3$:Eu^{2+} phosphors are produced from (Ca,Eu)$AlSiH_x$ and (Sr,Ca,Eu)$AlSiH_x$ powder by the direct nitriding method using CaH_2 as the

flux even under atmospheric-pressure heating conditions. In order to remove residual oxygen, CaH_2 powder properly additive on the (Ca,Eu)$AlSiH_x$ and (Sr,Ca,Eu)$AlSiH_x$ intermetallic alloys and it gives very positive effect to reduce oxygen contents. The usability of hydride alloy material and the lower cost may be suitable for the mass production of this phosphor.

The samples doped with Eu^{2+} ion at the optimized concentration of 3 at% (*vs.* alkaline earth atom) is efficiently excited by the blue light (400 – 470 nm) and give the emission peaking at 650 nm for $Ca_{1-x}Eu_xAlSiN_3$. Particularly, the emission band of $(Sr_{0.42}Ca_{0.56})AlSiN_3:Eu^{2+}$(2 at%) phosphor (644 nm) shifts to the red isochromatic region around 615 nm with increasing the Sr content. In future, the Ca content of $(Sr,Ca)AlSiN_3:Eu^{2+}$ phosphors should be much reduced by optimizing the composition of (Sr,Ca)$AlSiH_x$ precursor and the heating condition to produce the $(Sr,Ca)AlSiN_3:Eu^{2+}$ phosphors which have the emission bands in such red isochromatic region.

The obtained samples show low temperature quenching effect, as well as excellent chemical and thermal stabilities which enable an application of nitride phosphor to the red component of white LEDs, and white light with high CRI value can be obtained by coupling with a blue LED chip together with $YAG:Ce^{3+}$ phosphor.

References

[1] O. J. Rubio, *J. Phys. Chem. Solids.*, **521** (1991) 101.

[2] S. Lizzo, A. Meijerink, G. Blasse, *J. Lumin.*, **59** (1994) 185.

[3] R. J. Xie, N. Hirosaki, M. Mitomo, K. Uheda, T. Suehiro, X. Xu, Y. Yamamoto, T. Sekiguchi, *J. Phys. Chem. B*, **109** (2005) 9490.

[4] J. W. H. van Krevel, J. W. T. Rutten, H. Mandal, H. T. Hinzen, R. Metselaar, *J. Solid State Chem.*, **165** (2002) 19.

[5] N. Hirosaki, R. J. Xie, K.Kimoto, T. Sekiguchi, Y. Yamamoto, T. Suehiro, M. Mitomo, *Appl. Phys. Lett.*, **86** (2005) 211905.

[6] X. F. Song, H. He, R. L. Fu, D. L. Wang, X. R. Zhao, Z. W. Pan, *J. Phys. D: Appl. Phys.*, **42** (2009) 065409.

[7] Y. Q. Li, A. C. Delsing, G. de With, H. T. Hintzen, *Chem. Mater.*, **17** (2005) 3242.

[8] K. Uheda, N. Hirosaki, Y. Yamamoto, A. Naito, T. Nakajima, H. Yamamoto, *Electrochem.*

Solid-State Lett., **9** (2006) H22.

[9] H. Watanabe, N. Kijima, *J. Alloy Compd.*, **475** (2009) 434.

[10] H. A. Höppe, H. Lutz, P. Morys, W. Schnick, A. Seilmeier, *J. Phys. Chem. Solids*, **61** (2000) 2001.

[11] N. Hirosaki, K. Uheda, *Japanese Patent*, (2005) P2005-336253A.

[12] K. M. Sparta, R. Mueller, M. Merz, G. Roth, P. Adelmann, T. Wolf, *Acta Cryst. B*, **62** (2006) 710.

[13] M. Imai, K. Nishida, T. Kimura, H. Abe, *Appl. Phys. Lett.*, **80** (2002) 1019.

[14] D. Kuramoto, H.-S. Kim, T. Horikawa, M. Itoh, K. Machida, *J. phys.: conf. Ser.*, **379** (2012) 012015.

[15] A. G. Merzhanov, A. S. Rogachev, *Pure Appl. Chem.*, **64** (1992) 941.

[16] J. Li, T. Watanabe, H. Wada, T. Setoyama, M. Yoshimura, *Chem. Mater.*, **19** (2007) 3592.

[17] J. Li, T. Watanabe, N. Sakamoto, H. Wada, T. Setoyama, M. Yoshimura, *Chem. Mater.*, **20** (2008) 2095.

[18] B. Dierre, T. Takeda, T.Sekiguchi, T. Suehiro, K. Takahashi, Y. Yamamoto, R. J. Xie, N. Hirosaki, *Sci. Technol. Adv. Mater.*, **14** (2013) 064201.

[19] H. S. Kim, K. Machida, T. Horikawa, H. Hanzawa, *Chem. Lett.*, **43** (2014) 533.

[20] H. Watanabe, H. Wada, K. Seki, M. Itou, N. Kijima, *J. Electrochem. Soc.*, **155** (2008) F31.

[21] H. Watanabe, N. Kijima, *J. Ceram. Soc. Japan*, **117** (2009) 115.

[22] H. Watanabe, H. Yamane, N. Kijima, *J. Solid State Chem.*, **181** (2008) 1848.

[23] H. Watanabe, M. Imai, N. Kijima, *J. Am. Ceram. Soc.*, **92** (2009) 641.

[24] T. Watanabe, K. Nonaka, J. W. Li, K. Kishida, M. Yoshimura, *J. Ceram. Soc. Japan*, **120** (2012) 500.

[25] Y.-S. Kim, S.-W. Choi, J.-H. Park, E. Bok, B.-K. Kim, S.-H. Hong, *ECS J. Solid State Sci. Technol.* 2 (2013) R3021.

[26] M. Kubus, H.-J. Meyer, *Z. Anorg. Allg. Chem.* 639 (2013) 669.

[27] X. Q. Piao, T. Horikawa, H. Hanzawa, K. Machida, *J. Electrochem. Soc.* 153 (2006) H232.

Chapter 2

Carbothermal Reduction Characteristics of Alkaline Earth Carbonates, Formates and Acetates for Producing $CaAlSiN_3:Eu^{2+}$ Phosphor

2.1 Introduction

Until now, metal nitride precursor was used as an efficient reacting agent for the synthesis of red $M_{2-x}Eu_xSi_5N_8$ (M = Ca, Ba, Sr) [1-4], $Ca_{1-x}Eu_xAlSiN_3$ [5-6] and yellow-orange $Ca_{1-x}Ce_xAlSiN_3$ [7] phosphors. However, metal nitride precursor is unstable in air and sensitive in moisture. Also, they are expensive compared with that of metal carbonate and metal oxide precursor. Fig. 2-1 shows the emission intensity of $M_{2-x}Eu_xSi_5N_8$ (M = Ca, Sr, Ba) and $Ca_{1-x}Eu_xAlSiN_3$ phosphors compared with YAG:Ce^{3+} phosphor. For the $M_{2-x}Eu_xSi_5N_8$ (M = Ca, Sr) phosphor, caborthermal reduction and nitridation (CRN) method is very effective to get high intense emitting phosphor by using metal carbonate and metal oxide precursor with graphite reducing agent. However, CRN method is not effective for the $Ba_{2-x}Eu_xSi_5N_8$, $Ca_{1-x}Eu_xAlSiN_3$ phosphor, because the strong affinity of Ba^{2+} ions to O^{2-} will make reduction to be impossible to occur at low temperature. Also, in this method, residual carbon became a hindrance in obtaining higher emission intensity, so the 2nd treatment is required to remove carbon impurity.

Novel reducing agents, such as $C_3H_6N_6$, $C_2H_4N_4$, or $Sr(CH_3COO)_2$ were used to prepare $Sr_{2-x}Eu_xSi_5N_8$ [8] phosphor instead of carbon powder. From these precursors, molecular carbon species were generates during its decomposition time, and such molecular carbon is expected to be dispersed more homogeneously throughout the raw material. Therefore, the reduction will be performed more effectively compared to that performed by the conventional CRN route which uses solid carbon powder.

Meanwhile, the $CaAlSiN_3:Eu^{2+}$ phosphors prepared from the carbothermal reduction and nitridation (CRN) method by using $CaCN_2$ as a reducing agent as well as Ca source [9]. However, in this method, residual carbon became a hindrance in obtaining higher emission intensity. Therefore, new reducing agents and synthesis routes are still under investigation.

In this chapter, we synthesized the $CaAlSiN_3:Eu^{2+}$ (3 at%) phosphors by employing reducing agent, $Ca(HCOO)_2$ or $Ca(CH_3COO)_2$, were used as novel reducing agents instead of carbon powder. Calcium acetate generates molecular carbon during its own decomposition, and such molecular carbon is expected to be dispersed more homogeneously throughout the raw material. Thus, the reduction will be performed more effectively compared to that performed by the conventional CRN route which uses solid carbon powder. The effectiveness of this agent and the luminescent properties of the obtained phosphors were investigated for the application as a red phosphor for white LEDs.

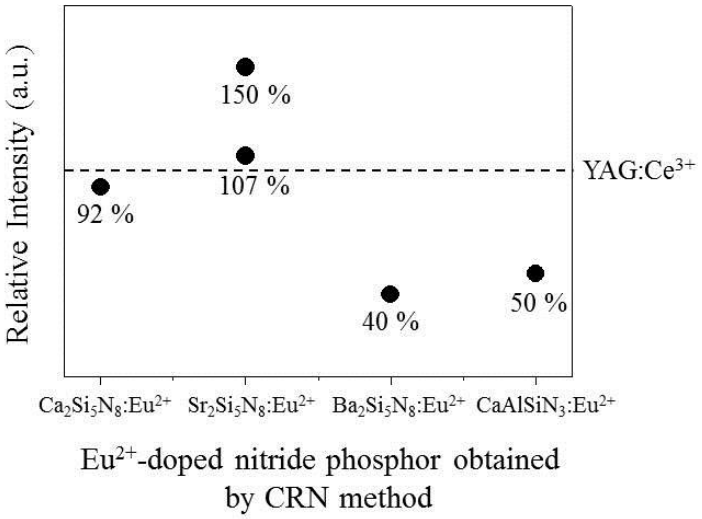

Fig. 2-1. Relative emission intensity of Eu^{2+}-doped nitride phosphors compared with $YAG:Ce^{3+}$ phosphor.

2.2 Experimental Section

The samples of $CaAlSiN_3:Eu^{2+}$ were synthesized from the mixtures which an appropriate amount of $(Ca_{1-x}Eu_{2x})CO_3$ ($CaCO_3Eu^{3+}$), Si_3N_4 (99.5%), and AlN (99.99%) was mixed stoichiometrically with $CaCO_3$ (1 : 0 with C, route 1), or $Ca(HCOO)_2$ (3 : 1 with $CaCO_3$, route 2), or $Ca(CH_3COO)_2$ (3 : 1 with $CaCO_3$, route 3), or $CaCO_3$ (1 : 1 with C, route 4), respectively. The mixed carbonate $CaCO_3:Eu^{3+}$ was co-precipitated from a nitrate acid solution of $CaCO_3$ (99.5%) and Eu_2O_3 (> 99.99%) by adding with another solution of $(NH_4)_2CO_3$ and then dried in vacuo. Each raw material was weighted stoichiometrically according to the formula of $Ca_{1.2-x}Eu_xAlSiN_3$

(x = 0.02 - 0.1) and mixed thoroughly in the glove box which was filled with a purified argon gas. The powder mixture was transferred into a covered-BN crucible and quickly loaded into a radio frequency furnace (Graphite heater). The furnace chamber was evacuated and filled with purified nitrogen. The mixture was heated at 900^{o}C for 2 h to decompose $CaCO_3$ completely, and then the temperature was raised to 1600^{o}C and kept for 5 h to form the $Ca_{1.2-x}Eu_xAlSiN_3$ powders. The phosphors were cooled in the furnace and finally target materials were obtained. All the heating processes were performed in a flowing nitrogen atmosphere (50 ml/min). In order to remove impurity phases, the prepared samples were washed by a hydrochloric acid solution. At last, the samples were dried in the oven for several hours, and then taken out for analysis.

Powder X-ray diffraction (XRD) measurements for $CaAlSiN_3:Eu^{2+}$ phosphors were carried out on a RIGAKU RINT2200 diffractometer using CuKα radiation. The lattice parameters and cell volumes were calculated from the recorded XRD patterns by using a DICVOL software [10] and Rietveld refinements were performed by a FULLPROF SUITE software [11-12] using a pseudo-Voigt function as a peak shape. For the Rietveld analysis, the XRD patterns were measured with a scanning step of 0.02^{o}/s in a 2θ range from 10 to 90^{o}. The oxygen and nitrogen analysis was made by a HORIBA EMGA-550 oxygen/nitrogen analyzer. The morphology of $CaAlSiN_3:Eu^{2+}$ powders were observed on a scanning electron microscope (SEM, HITACHI S-3000). The photoluminescence spectra of resultant phosphor powders were measured at room temperature by a HITACHI F-4500 fluorescence spectrometer and the spectra was obtained in a range of 200 ~ 800 nm with a scanning speed of 240 nm/min. For the comparing luminescence property, commercially available $YAG:Ce^{3+}$ (P46-Y3) powders were used.

2.3 Result and Discussion

Figures 2-2 shows typical XRD patterns of the $CaAlSiN_3:Eu^{2+}$ (3at %) phosphors prepared from the corresponding raw material mixtures : (a) $CaCO_3$, AlN and Si_3N_4 (= 1.18 : 0.8 : 1/3), (b) $CaCO_3$, $Ca(HCOO)_2$, AlN and Si_3N_4 (= 0.2925 : 0.8925 : 0.8 : 1/3), (c) $CaCO_3$, $Ca(CH_3COO)_2$, AlN and Si_3N_4 (= 0.2925 : 0.8925 : 0.8 : 1/3), and (d) $CaCO_3$, AlN, Si_3N_4 and C (= 1.185 : 0.8 : 1/3 : 1.2), where the commercial values in parenthesis represented the molar ratios. The reflection peaks of the $CaAlSiN_3:Eu^{2+}$ phosphor were well assigned based on a reference data (JCPDS

card : 39-0747). In case of $CaAlSiN_3:Eu^{2+}$(3 at%) phosphor prepared from $CaCO_3$ (a) and $CaCO_3$/C-based mixture (d) shows large amount of impurity phase such as AlN which were usually decreasing emission intensity of $CaAlSiN_3:Eu^{2+}$ phosphor. However, although $CaAlSiN_3:Eu^{2+}$(3 at%) phosphor prepared from $CaCO_3/Ca(HCOO)_2$ (0.2925 : 0.8925)-based mixture (b) and $CaCO_3/Ca(CH_3COO)_2$ (0.405 : 0.795)-based mixture (c) shows no AlN impurity phase and from this route, all reflection peaks were well indexed to the single phase of $CaAlSiN_3$ which was previously reported one [13-16], It indicates that the sample (c) has an orthorhombic structure (*Cmc2₁*) and the lattice parameters *a*, *b* and *c* are calculated to be 9.730(2), 5.645(1) and 5.046(4) Å, with cell volume 277.18 $Å^3$. The atomic coordinates and thermal parameters of sample (c) are given in Table 1. In accordance with the space group, Al and Si atoms randomly distribute at 8b site. In addition, there was no observing other second-phases such as CaO and $Ca(OH)_2$ even use of excess amount of Ca component.

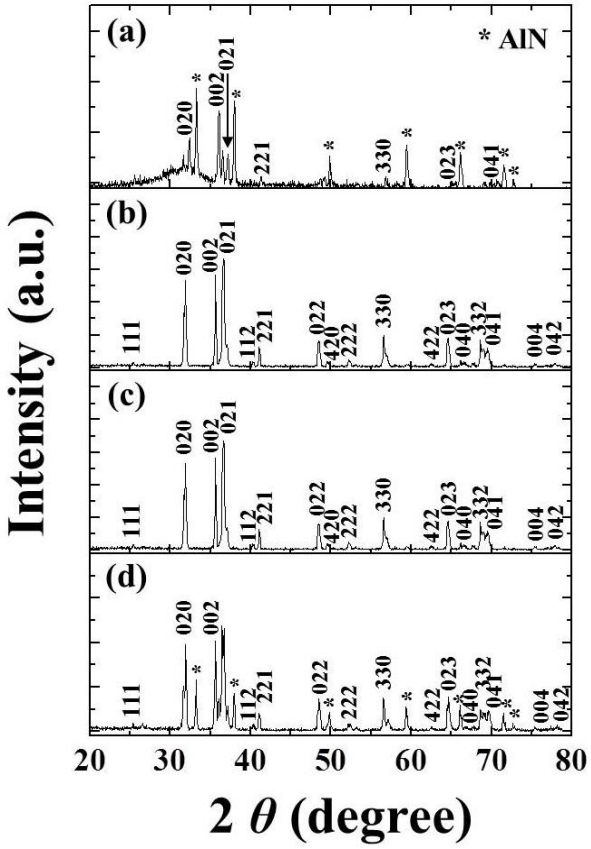

Fig. 2-2. . XRD patterns of $CaAlSiN_3:Eu^{2+}$(3 at%) phosphor prepared from raw material mixture : (a) $CaCO_3$, AlN and Si_3N_4 (= 1.185 : 0.8 : 1/3), (b) $CaCO_3$, $Ca(HCOO)_2$, AlN and Si_3N_4 (=

0.2925 : 0.8925 : 0.8 : 1/3), (c) $CaCO_3$, $Ca(CH_3COO)_2$, AlN and Si_3N_4 (= 0.2925 : 0.8925 : 0.8 : 1/3), and (d) $CaCO_3$, AlN, Si_3N_4, and C (= 1.185 : 0.8 : 1/3 : 1.2), respectively.

Table 2-1. Atomic coordinates and isotropic displacement parameters for the $CaAlSiN_3:Eu^{2+}$(3 at%)

Atom	Site ($Cmc2_1$)	Coordinates			U_{iso} (Å^2)
		x	*y*	*z*	
Ca,Eu	4a	0	0.3144(2)	0.9746(7)	0.0163(9)
Al/Si	8b	0.1712(2)	0.8424(1)	0.0484(3)	0.0032(2)
N(1)	8b	0.2083(7)	0.8727(3)	0.4061(4)	0.0003(5)
N(2)	4a	0	0.2305(3)	0.5000(5)	0.0004(9)

[a] R_p = 17.1 %, R_{wp} = 15.5 %, R_{exp} = 17.0 %.

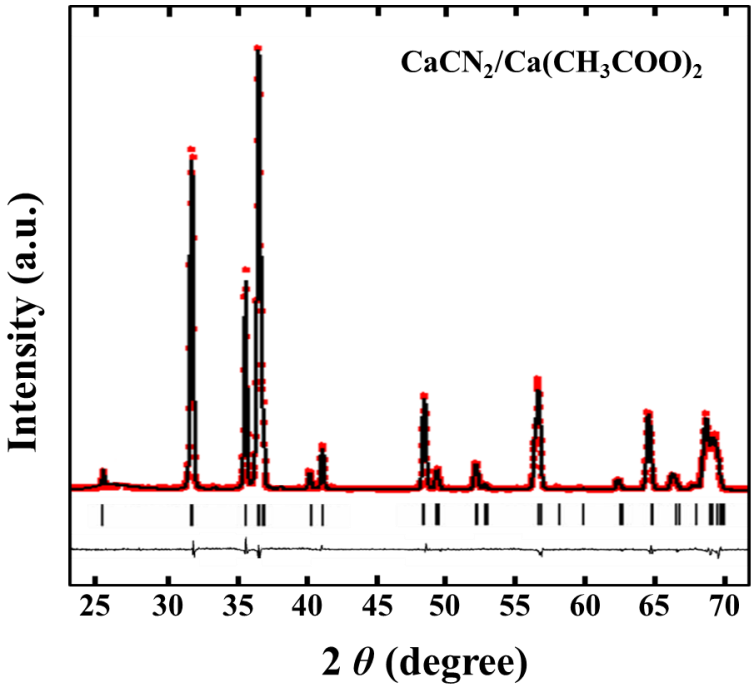

Fig. 2-3. Differential profile between the observed (circle) and calculated (line) XRD patterns for the $CaAlSiN_3:Eu^{2+}$(3 at%) phosphor prepared from $CaCO_3/Ca(CH_3COO)_2$-based mixture. The atomic coordinates and thermal parameters listed in Table 2-1 were used for the evaluation.

The differential profile between the observed and calculated XRD patterns for the $CaAlSiN_3:Eu^{2+}$(3 at%) phosphor prepared from $CaCO_3/Ca(CH_3COO)_2$ (0.2925 : 0.8925)-based mixture is shown in Fig. 2-3. One can see that the observed pattern is in good accordance with the calculated one due that the differential profile between these is so flat. This means that the $CaAlSiN_3:Eu^{2+}$ powders prepared from $CaCO_3/Ca(CH_3COO)_2$ (0.2925 : 0.8925)-based mixture scarcely contain any impurity such as AlN (see Figs. 1(c)). At a high temperature sintering, to account for the reduction of metal oxide, some reducing species, such as CH_3 or amorphous carbon must be formed. Under the strong reducing atmosphere, CaO and Eu_2O_3 are reduced to the corresponding metals, and simultaneously, they were completely nitrogenized and then reacted with the silicon nitride. Therefore, the $Ca(CH_3COO)_2$ serve as efficient reducing agents as well as Ca source to prepare such nitride phosphors.

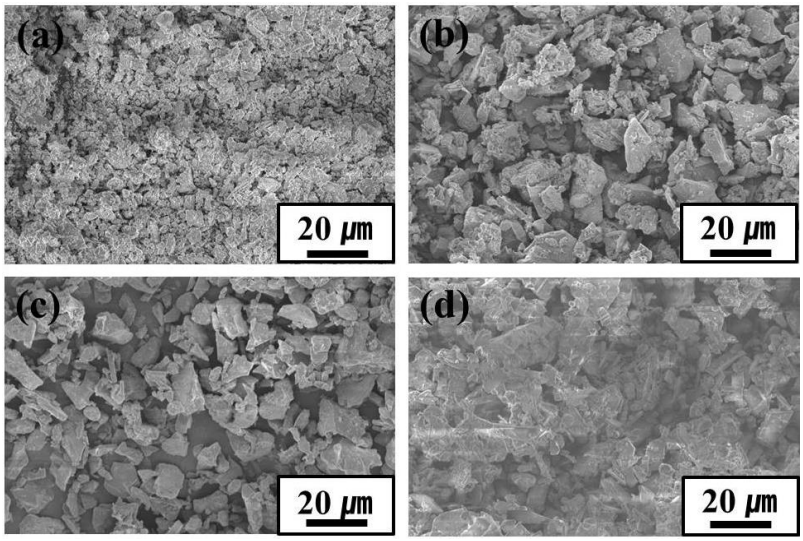

Fig. 2-4. SEM images of $CaAlSiN_3:Eu^{2+}$(3 at%) phosphor given in Fig. 2-1.

The typical SEM images of the $CaAlSiN_3:Eu^{2+}$(3 at%) phosphors obtained via $CaCO_3$ mixed with various reductant (a): no reductant, (b): $Ca(HCOO)_2$, (c): $Ca(CH_3COO)_2$, and (d): C were shown in Fig. 2-4, respectively. The phosphor obtained from $CaCO_3/Ca(CH_3COO)_2$(0.39 : 0.78)-based mixture shows angled-shape compared with that of sample (a), (d) and the mean size of the phosphor is about 20 μm, and the phosphor contains irregular particles with the clear surface. Although the uniform morphology is not obtained, it is acceptable for the white LEDs

application as the particle size requirement is not as strict as that in the plasma display panel (PDP) field.

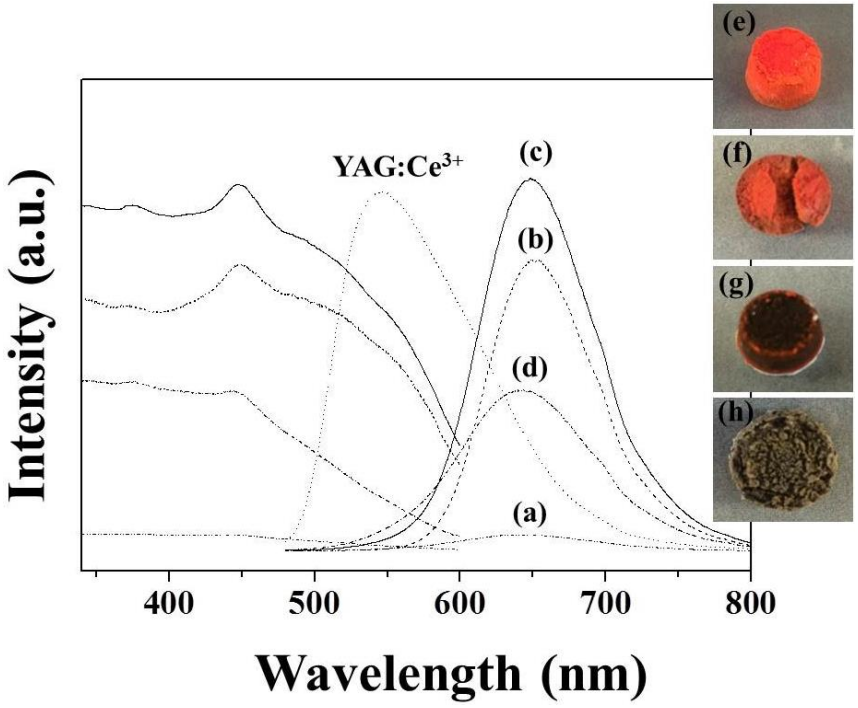

Fig. 2-5. PL spectra of the $CaAlSiN_3:Eu^{2+}$(3 at%) phosphors prepared from raw material mixture : (a) $CaCO_3$, AlN and Si_3N_4, (= 1.185 : 0.8 : 1/3), (b) $CaCO_3$, $Ca(HCOO)_2$, AlN and Si_3N_4 (= 0.2925 : 0.8925 : 0.8 : 1/3), (c) $CaCO_3$, $Ca(CH_3COO)_2$, AlN and Si_3N_4 (= 0.2925 : 0.8925 : 0.8 : 1/3), and (d) $CaCO_3$, AlN, Si_3N_4, and C (= 1.185 : 0.8 : 1/3 : 1.2), respectively, together with that of $YAG:Ce^{3+}$ (PY46-3) phosphor as a reference. Right side inset figures (e), (f), (g), and (h) shows the photograph of samples (c), (b), (d), and (a), respectively.

The photoluminescence spectra of the $CaAlSiN_3:Eu^{2+}$(3 at%) phosphor prepared from raw material: (a) $CaCO_3$ only, (b) $CaCO_3$/$Ca(HCOO)_2$-based mixture, (c) $CaCO_3$/$Ca(CH_3COO)_2$-based mixture, and (d) $CaCO_3$/C-based mixture, respectively, together with that of $YAG:Ce^{3+}$ (P46-Y3) standard phosphor is shown in Fig 2-5. The broad excitation spectra consist of two broad bands covering the wavelength range from UV to visible region. The strong absorption in the range of 350–600 nm are dominantly assigned to the electronic transition of the Eu^{2+} ions ($4f^7 \rightarrow 4f^6 5^d$). It worth noting that the strong absorption in the range of 400–600 nm matches perfectly with the

current Ga(In)N LED chips, which indicating a potential application as the down-conversion phosphors. The photographs of phosphor body are shown in Fig. 2-5 as an inset: (h) $CaCO_3$ only, (f) $CaCO_3/Ca(HCOO)_2$-based mixture, (e) $CaCO_3/Ca(CH_3COO)_2$-based mixture, and (g) $CaCO_3$/C-based mixture, respectively. The phosphors with bright orange body color were obtained from $CaCO_3/Ca(HCOO)_2$-based mixture and $CaCO_3/Ca(CH_3COO)_2$-based mixture, respectively. However, for the sample prepared from $CaCO_3$ only and $CaCO_3$/C-based mixture shows gray-dark orange body color resulting from poor reactivity. For the sample prepared from $CaCO_3/Ca(CH_3COO)_2$-based mixture (c), the emission spectrum at the excitation of 450 nm shows a broad band peaking at 650 nm which is assigned to the allowed $4f^65d^1 \rightarrow 4f^7(^8S_{7/2})$ transition of Eu^{2+} ion. Compared with alkaline fluoride $MF_2:Eu^{2+}$ [17] or silicate $M_2SiO_4:Eu^{2+}$ (M=Sr/Ba) [18], the emission of $CaAlSiN_3:Eu^{2+}$ phosphor occurs at fairly longer wavelength. It was attributed to the higher electronegativity and nephelauxetic effect of N^{3-} ion, which effectively lower the gravity center of 5d orbitals of Eu^{2+} ion. The emission intensity of phosphors prepared form $CaCO_3/Ca(CH_3COO)_2$-based mixture was about 92% of $YAG:Ce^{3+}$ (P46-Y3) at the same excitation of 450 nm. In the Table 2-2, their luminescence properties are arranged with O/N contents. The peak wavelength shows red-shifting when oxygen content decreases. It is known that in nitride phosphors, the high electronegativity and strong covalent bondings between Eu and N atoms effectively lower the gravity center of 5*d* orbitals of Eu^{2+} (nephelauxetic effect), and this low oxygen containing phosphor shows red emission in long wavelength region.

Table 2-2. Luminescence properties and O/N contents for the $CaAlSiN_3:Eu^{2+}$(3 at%) phosphors with various reductant

Samples	Raw materials[a)]	λ_{em} (nm)	λ_{ex} (nm)	R. I. (%)[b)]	O (wt%)	N (wt%)
(a)	$CaCO_3$	450	644	5	15.85	19.14
(b)	$CaCO_3 + Ca(HCOO)_2$	450	650	67	0.89	27.17
(c)	$CaCO_3 + Ca(CH_3COO)_2$	450	650	93	0.71	29.33
(d)	$CaCO_3$ + C	450	644	47	7.32	21.48

[a)] The raw materials were mixed with AlN, $1/3Si_3N_4$, $1/2Eu_2O_3$.

[b)] The values were based on that of $YAG:Ce^{3+}$ (100%).

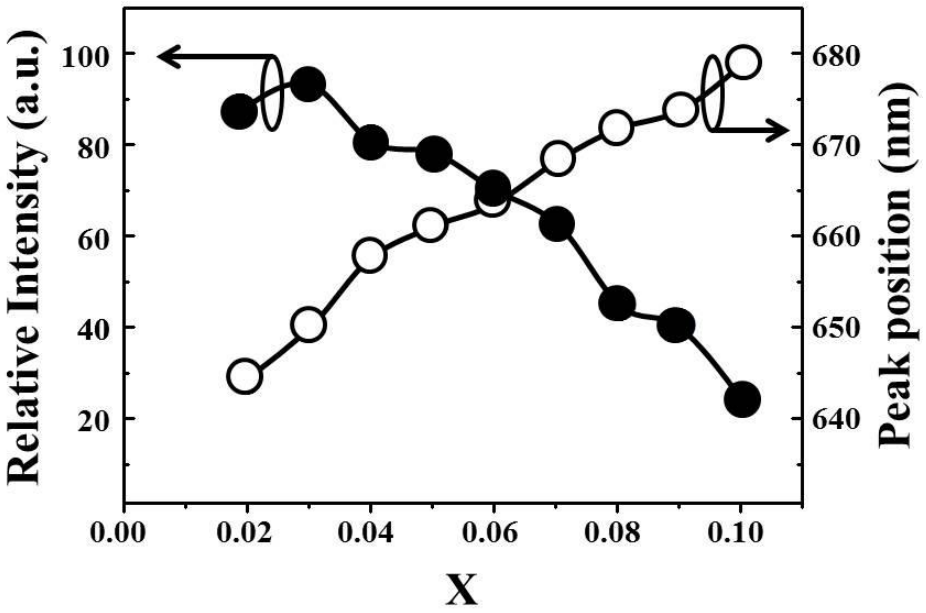

Fig. 2-6. Dependences of the Eu^{2+} concentration on the emission intensity and peak position of the $CaAlSiN_3:Eu^{2+}$ phosphors prepared from the $CaCO_3/Ca(CH_3COO)_2$-based mixtures containing 0.8AlN, $1/3Si_3N_4$, and 0.01 ~ 0.05 Eu_2O_3.

The photoluminescence characteristics of the $(Ca_{1.2-x}Eu_x)AlSiN_3:Eu^{2+}$ phosphor prepared from $CaCO_3/Ca(CH_3COO)_2$-based mixture with a changing of Eu^{2+} concentration (x = 0.02 - 0.10) is shown in Fig. 2-6. The emission intensity is supposed to be proportional to the activator amount in an ideal situation. However, there is always a critical concentration of activator, at which the emission intensity begins to decrease. This decrease can be ascribed by the concentration quenching which is mainly caused by a non-radiative energy transfer between two Eu^{2+} ions in the host lattice. In this work, with increasing Eu^{2+} ion content, the emission intensity is maximized at 3 at% of Eu^{2+} ion and then decreases slowly. At the same time, the emission peaks are shifted to the long wavelength when the Eu^{2+} concentration increases. This can be explained by the mismatch of ionic radius between the small Ca^{2+} and large Eu^{2+} in the lattice [19]. The mismatch cause some changes in the crystal field and resulting in the splitting of 5d level of Eu^{2+}. So, the possibility of energy transfer between higher 5d level and lower 5d level of Eu^{2+} ions may increase when the Eu concentration is increased. It is assumed that the high doping of Eu^{2+} ions reduces the emission energy, because the transition energy from higher 5d excited state to 4f ground state is larger than that of reverse case. Thus, the observed emission peak position of

$Ca_{1.2-x}Eu_xAlSiN_3$ (x = 0.02 - 0.10) phosphors shifts from 645 to 678 nm by increasing the Eu^{2+} contents.

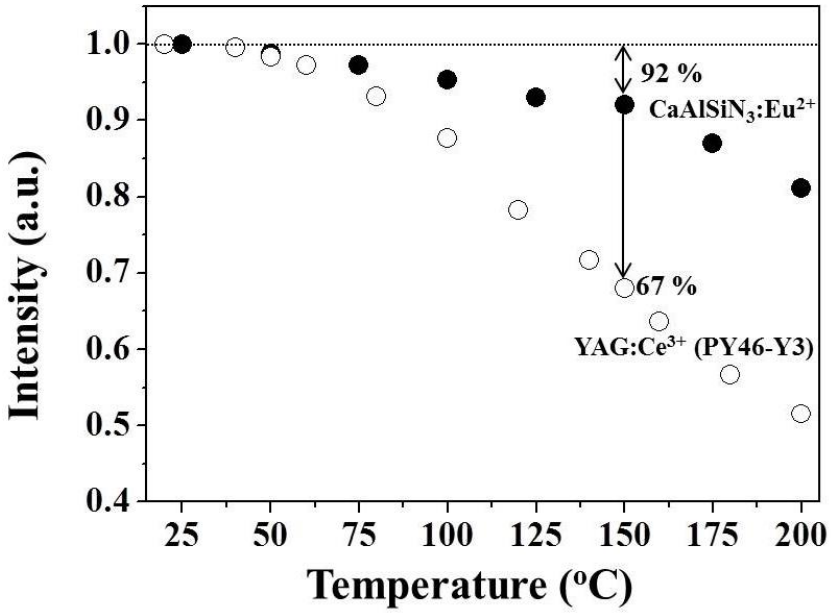

Fig. 2-8. Thermal quenching characteristics of the $CaAlSiN_3:Eu^{2+}$(3 at%) phosphors prepared from $CaCO_3/Ca(CH_3COO)_2$-based mixtures, together with that of YAG:Ce^{3+} (PY46-3) phosphor as the reference.

The temperature dependence of the normalized PL intensity of obtained $CaAlSiN_3:Eu^{2+}$(3 at%) phosphor prepared from $CaCO_3/Ca(CH_3COO)_2$-based mixture is shown in Fig. 2-8, together with that of YAG:Ce^{3+} (P46-Y3) phosphor. For the application of white LEDs, a temperature quenching behavior is one of the important parameters to evaluate the quality of a phosphor. When the temperature is increased to the working temperature of white LEDs (150°C), the emission intensity of $Ca_{1.2-x}Eu_xAlSiN_3$ (x = 0.03) phosphor against the excitation of 450 nm are about 92% of that at room temperature, respectively, and more stronger than that of YAG:Ce^{3+} sample (68% at 150°C). The thermal quenching mechanism is commonly explained as an electronic transition between the $4f^6$-5d and $4f^7$ states. In this work, $Ca_{1.2-x}Eu_xAlSiN_3$ (x = 0.03) phosphor has high quenching temperature and small stokes shift of the Eu^{2+} ion in the rigid host. As a nitride phosphor, this phosphor shows a low temperature quenching effect with high thermal stabilities.

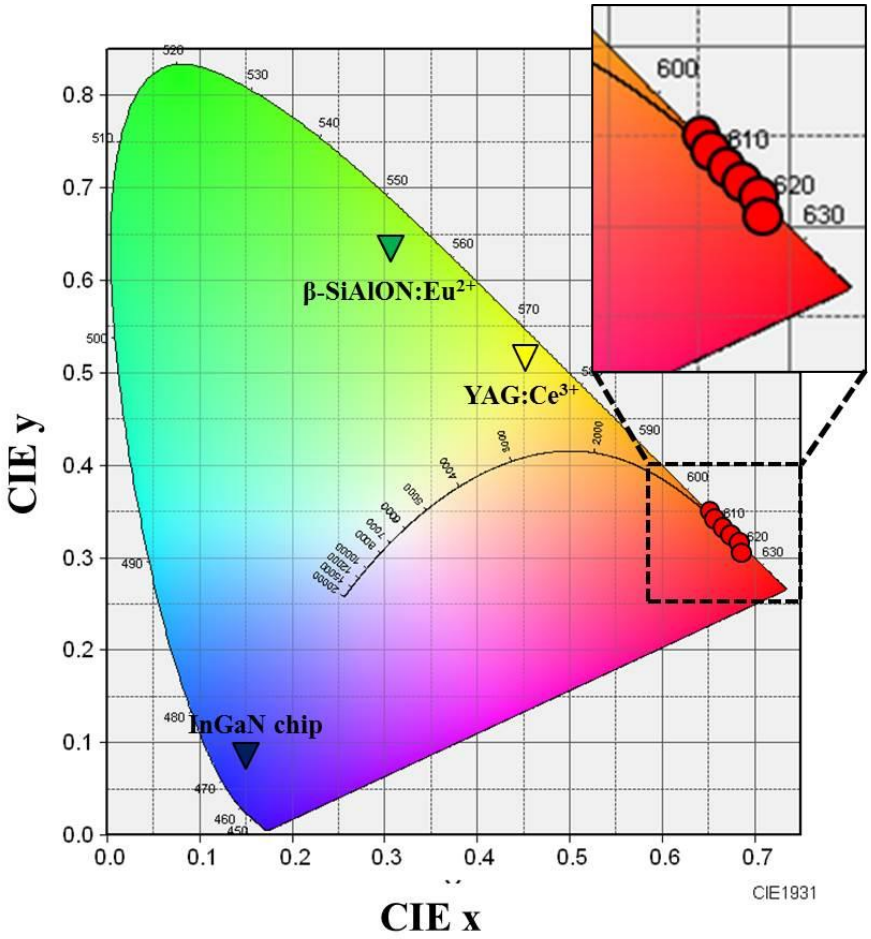

Fig. 2-9. CIE 1931 chromaticity coordinates of $Ca_{1.2-x}Eu_xAlSiN_3$ phosphors prepared from $CaCO_3/Ca(CH_3COO)_2$-based mixture.

The CIE (Commission Internationale del'Eclairage) color coordinates of $CaAlSiN_3:Eu^{2+}$(3 at%) phosphor prepared from $CaCO_3/Ca(CH_3COO)_2$-based mixture is given in Fig. 2-9. Along with an increasing Eu^{2+} ion concentration, the chromaticity coordinates (*x*, *y*) shifts from (0.653, 0.349) and (0.684, 0.303), respectively, while that of YAG:Ce^{3+} (P46-Y3) is measured to be (0.469, 0.533). As indicated, the saturation of the chromaticity of the present $CaAlSiN_3:Eu^{2+}$(3 at%) phosphors is high enough to compensate for red color component and it is shown that the efficient white light with high color rendering index (CRI) value can possibly be made by combining with a blue LED chip together with a proper amount of green phosphor.

2.4 Conclusions

Compared with the CRN method by using $CaCO_3$/C mixture powder, the molecular-type carbon species precursor nitriding method has two significant advantages: (1) As shown in XRD and PL data, single phase of $CaAlSiN_3$ is formed without any impurity phase and also the luminescence property is much improved compared with that of using solid carbon species precursor. Therefore, such molecular-type carbon species in $Ca(CH_3COO)_2$ is effective to take place the carbothermal reduction and nitriding. (2) The $CaAlSiN_3:Eu^{2+}$ phosphor prepared from the $CaCO_3$/$Ca(CH_3COO)_2$-based mixtures shows fine particles with the mean size of 20 μm. This suggest that the reactivity of $Ca(CH_3COO)_2$ reductant is best to form the $CaAlSiN_3$ crystal lattice even under such atmospheric pressure heating conditions.

The strong emission peaking at 650 nm with the saturated chromaticity coordinates and low thermal quenching effect shows that this efficient red phosphor can be used as a potential candidate for the phosphor-converted white LEDs.

References

[1] M. G. Craford, "Commercial Light Emitting Diode Technology", Kluwer, Dordrecht, (1996).

[2] K. Uheda, N. Hirosaki, Y. Yamamoto, A. Naito, T. Nakajima, H. Yamamoto, *Electrochem. Solid-state Lett.*, **9** (2006) H22.

[3] X. Piao, K. Machida, T. Horikawa, H. Hanzawa, Y. Shimomura, N. Kijima, *Chem. Mater.*, **19** (2007) 4592.

[4] J. Li, T. Watanabe, H. Wada, T. Setoyama, M. Yoshimura, *Chem. Mater.*, **19** (2007) 3592.

[5] R. Xie, N. Hirosaki, *Sci. Tech. Adv. Mater.*, **8** (2007) 588.

[6] J. Li, T. Watanabe, N. Sakamoto, H. Wada, T. Setoyama, M. Yoshimura, *Chem. Mater.*, **20** (2008) 2095.

[7] H. Watanabe, H. Wada, K. Seki, M. Itou, N. Kijima, *J. Electrochem. Soc.*, **155** (2008) F31.

[8] H. A. Höppe, H. Lutz, P. Morys, W. Schnick, and A. Seilmeier, *J. Phys. Chem. Solids.*, **61** (2000) 2001.

[9] H. S. Kim, K. Machida, T. Horikawa, and H. Hanzawa, *Chem. Lett.*, **43** (2014) 533.

[10] A. Boultif, D. Louer, *J. Appl. Cryst.*, **37** (2004) 724.

[11] J. Rodr´ıguez-Carvajal, *Physica B*, **192** (1993) 55.

[12] T. Roisnel, J. Rodr´ıguez-Carvajal, *Mater. Sci. Forum*, **378** (2001) 118.

[13] N. Hirosaki, K. Uheda, *Japanese Patent*, (2005) P2005.

[14] J. Li, T. Watanabe, H. Wada, T. Setoyama, M. Yoshimura, *Chem. Mater.*, **19** (2007) 3592.

[15] J. Li, T. Watanabe, N. Sakamoto, H. Wada, T. Setoyama, M. Yoshimura, *Chem. Mater.*, **20** (2008) 2095.

[16] B. Dierre, T. Takeda, T.Sekiguchi, T. Suehiro, K. Takahashi, Y. Yamamoto, R. J. Xie, N. Hirosaki, *Sci. Technol. Adv. Mater.*, **14** (2013) 064201.

[17] D. B. Gatch, D. M. Boye, Y. R. Shen, M. Grinberg, Y. M. Yen, R. S. Meltzer, *Phys. Rev. B*, **74** (2006) 195117.

[18] J. K. Park, K. J. Choi, C. H. Kim, H. D. Choi, S. Y. Park, *Electrochem. Solid-State Lett.*, **7** (2004) H15.

[19] R. D. Shannon, *Acta Crystallogr., Sect. A: Cryst. Phys., Diffr., Theor. Gen. Crystallogr.*, **32** (1975) 751.

Chapter 3

Carbothermal Reduction Synthesis using $CaCN_2$ as Calcium and Carbon Sources for $CaAlSiN_3:Eu^{2+}$ Phosphor and Their Luminescence Properties

3.1. Introduction

Metal nitride/oxynitride phosphors, e.g. the Eu^{2+} doped phosphors such as α- and β-SiAlON [1,2], $M^{II}_2Si_5N_8:Eu^{2+}$ (M^{II} = Ca, Sr, Ba) [3-6], $LaSi_3N_5:Eu^{2+}$ [7], and $CaAlSiN_3:Eu^{2+}$ [8-10] of which the host lattices consist of covalently bonded MX_4 (M=Si,Al; X=N,O) tetrahedral units show excellent luminescence and low thermal quenching properties together with good chemical stability [11-13]. Also, they have the strong absorption bands in the UV-visible spectral range and give broad emission spectra covering red and/or green color regions that allow them to be used as the down-conversion phosphors for the white LED modules.

For last several years, the $CaAlSiN_3:Eu^{2+}$ phosphor has been noted among the nitride phosphors, due to the excellent luminescence properties of red color, especially its low thermal quenching characteristics. However, critical preparation conditions, viz. high temperature and pressure up to 2000°C and 1 MPa, are generally required to synthesize high-quality $CaAlSiN_3:Eu^{2+}$ phosphor from Ca_3N_2, AlN, Si_3N_4, and EuN. Among of these starting materials, Ca_3N_2 and EuN are deliquescent and furthermore highly coasted [10]. Consequently, from the viewpoint to use this phosphor in the wider application fields, novel synthesis method for producing the high-performance $CaAlSiN_3:Eu^{2+}$ phosphor is strongly required and the present authors have proposed the efficient method using metal hydrides as the precursors for the nitride phosphors [14]. However, these metal hydrides are too reactive to use as the main raw material at a mass production level.

Meanwhile, the carbothermal reduction and nitridation (CRN) method using C (graphite) as a reductant has employed to synthesized $Sr_2Si_5N_8:Eu^{2+}$ [5], $Ca_2Si_5N_8:Eu^{2+}$ [6], and Ca-α-$SiAlON:Eu^{2+}$ [15] phosphors. However, the resultant phosphors still contain the residual carbon which lowers the emission intensity because such carbon species are usually colored and thus absorb the blue lights generated from Ga(In)N LEDs. For the $CaAlSiN_3:Eu^{2+}$ phosphor, the CRN method is not

suitable for producing these from the raw materials, $CaCO_3:Eu^{3+}$, AlN, Si_3N_4, and C because the impurity phases of AlN and carbon residues are inevitably remained in the resultant materials. However, the present authors have recently succeeded in synthesizing the $CaAlSiN_3:Eu^{2+}$ phosphor in an almost single phase by the improved CRN method using $CaCN_2$ as the Ca source and reduction reagent even under the normal-pressure heating condition [16].

In this work, the reaction mechanism of the above-mentioned CRN method for producing the $CaAlSiN_3:Eu^{2+}$ phosphor was systematically studied as well as the optimization of their synthesis conditions. Consequently, the high-quality powders of $CaAlSiN_3:Eu^{2+}$ phosphors were synthesized from the inorganic raw materials, e.g. $CaCN_2$, $CaCO_3:Eu^{3+}$, AlN, and Si_3N_4 under the ambient pressure heating conditions with a high reproducibility.

3.2. Experimental Section

The samples of $CaAlSiN_3:Eu^{2+}$ were synthesized from raw materials of $CaCN_2$ (Tokyo-kasei, 99%), $CaCO_3$ (Wako, 99.99%), AlN (Wako, 99.99%), Si_3N_4 (Nilaco, 99.5%), and Eu_2O_3 (Shin-Etsu, 99.99%). Among them, appropriate amounts of $(1-x)CaCO_3$ and xEu_2O_3 were weighted and preliminary dissolved in a NH_3 solution and by adding a NH_4CO_3 solution, mixed carbonates, $CaCO_3:Eu^{3+}$(x at%)($Ca_{1-x}Eu_xCO_3$), were precipitated and filtered. After drying, the carbonate powders were used as the raw materials for Ca and Eu components. The raw materials $CaCN_2$, $CaCO_3:Eu^{3+}$, AlN, and Si_3N_4 were weighted stoichiometrically according to nominal formula of $Ca_{1.2-x}Eu_xAlSiN_3$ (x = 0.02 - 0.1) and mixed thoroughly by using an agate mortar in air, where the molar ratios of $CaCN_2$ and $CaCO_3:Eu^{3+}$ for such mixtures were changed as follows: (a) 1.185 : 0, (b) 0.8325 : 0.3525, (c) 0.5925 : 0.5925, (d) 0.3525 : 0.8325, and (e) 0 : 1.185, respectively. Each mixture was placed in a covered-BN crucible and quickly loaded on the radio frequency furnace equipped with a graphite heater. The furnace chamber was evacuated and filled with a purified nitrogen gas. The mixture was heated at 1050°C for 2 h to take place the reaction between $CaCN_2$ and $CaCO_3:Eu^{3+}$ ($CaCN_2 + CaCO_3:Eu^{3+} + N_2 \rightarrow 2/3Ca_3N_2:Eu^{3+} + CO + CO_2$) preferentially and then the temperature was raised to 1600°C for reacting Ca_3N_2 with the other raw materials and kept for 5 h to form the purpose nitrides. They were cooled in the furnace and took out at room temperature. All the heating processes were performed in a flow (50 ml/min) of high purity N_2 gas

(99.999%) under ambient pressure condition. In order to remove impurity phases, the resulting nitride powders were washed by a hydrochloric acid solution. The total reaction is expressed as follows:

$$1/2(1-x)CaCN_2 + 1/2(Ca_{1-x}Eu_{2x})CO_3 + yAlN + 1/3Si_3N_4 \rightarrow (Ca_{1-x}Eu_x)Al_ySiN_3 + CO_2\uparrow \quad (1)$$

For the stoichiometric mixture of raw materials, the resultant samples contained the unreacted AlN phase and, to minimize this amount, the *y* values for AlN in Eq. (1) was optimized in a rage of $y = 0.6 - 1.0$.

All samples were identified by a powder X-ray diffractometer (XRD, RINT2200, Rigaku) using Cu Kα (λ = 0.15405 nm) radiation operating at 40 kV and 30 mA with a scanning step of $0.02^o(2\theta)$. The powder samples were mounted on a flat plate holder by the side filling method to avoid the preferred orientation. The particle morphology of $CaAlSiN_3:Eu^{2+}$ powders were observed by a field emission scanning electron microscopy (FE-SEM; ERA-8800, ELIONIX) equipped with an energy dispersive X-ray (EDX) spectroscopy. The photoluminescence (PL) spectra were measured on a fluorescent spectrophotometer (F-4500, Hitachi) with a Xe lamp as an excitation source at room temperature. The oxygen and nitrogen contents were also measured on an oxygen/nitrogen analyzer (EMGA-550, Horiba) by an inert gas fusion method.

3.3 Result and Discussion

The carbothermal reduction and nitridation (CRN) is good process for producing $Sr_2Si_5N_8:Eu^{2+}$ and the other nitride phosphors without Al element in the host lattices. For $CaAlSiN_3:Eu^{2+}$ phosphor, the aluminum nitride (AlN) and graphite (C) used as the raw materials inevitably remains as impurity phases without performing any further reaction in the samples which are prepared according to the following scheme:

$CaCO_3:Eu^{3+} + AlN + Si_3N_4 + C\ (graphite) \rightarrow CaAlSiN_3:Eu^{2+}$ (in N_2, ~1600^{o}C, ~6h)

The resultant phosphors are usually colored with such AlN and C residues, that considerably depress the excitation by visible lights, e.g. the blue light generated by Ga(In)N-based LEDs. This is due that the reactivity of graphite is not enough for reducing the calcium oxide (CaO) derived from $CaCO_3$ to Ca_3N_2.

Calcium cyanamide, $CaCN_2$, consists of Ca^{2+} and $^{-}N=C=N^{-}$ ions, of which the organic (cyanamide) anion much more react with the CaO powder and the unreacted $CaCN_2$ residue should volatilize in a range of 1150 - 1200^{o}C (sublimation temperature) without forming any carbon residue. The present author have succeeded in synthesizing the $CaAlSiN_3:Eu^{2+}$ phosphor with excellent PL properties as a single phase.

The CRN process of Eq. (1) is schematically illustrated in Fig. 3-1. All the temperature above 800^{o}C, $CaCO_3$ is decomposed to CaO and then it reacts with $CaCN_2$ to form Ca_3N_2. However, in our previous work [16], no XRD pattern assigned to it was detected because Ca_3N_2 promptly react with the other raw materials, AlN and Si_3N_4. At the temperature around 1200^{o}C, the mixed phase of $CaAlSiN_3$ and AlN are produced but the unreacted portion of $CaCN_2$ volatilizes because T_B = 1150 - 1200^{o}C for it. Finally, the $CaAlSiN_3$ host lattice is mainly formed at the temperature around 1600^{o}C.

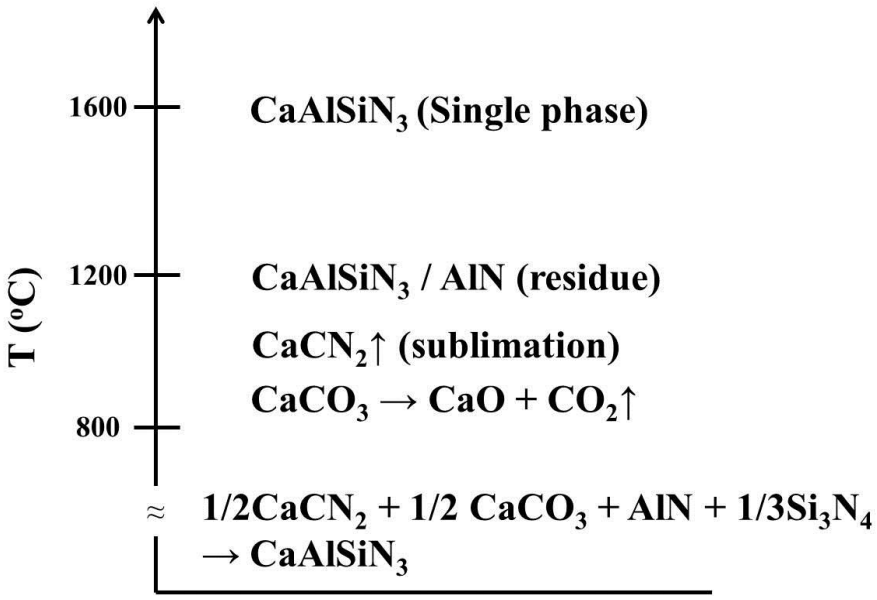

Fig. 3-1. A relationship between phase change and temperature.

Figure 3-2 shows the XRD patterns of $CaAlSiN_3:Eu^{2+}$(3 at%) phosphors prepared from the $CaCN_2/CaCO_3:Eu^{3+}$-based mixtures with various molar ratios of them. Generally, the Ca amount is 20% excess to the stoichiometric ones of the other raw materials (see Eq. (1)), since the excess amount of Ca element is converted to low melting material like Ca_3N_2 and served as a flux. The

XRD patterns were mainly assigned to the reflection peaks of $CaAlSiN_3$ host lattice (JCPDS card: 39-0747), but a trace amount of AlN (JCPDS card: 25-1133) which usually depressed the emission intensity of $CaAlSiN_3:Eu^{2+}$ phosphor was detected as an impurity phase on all the samples.

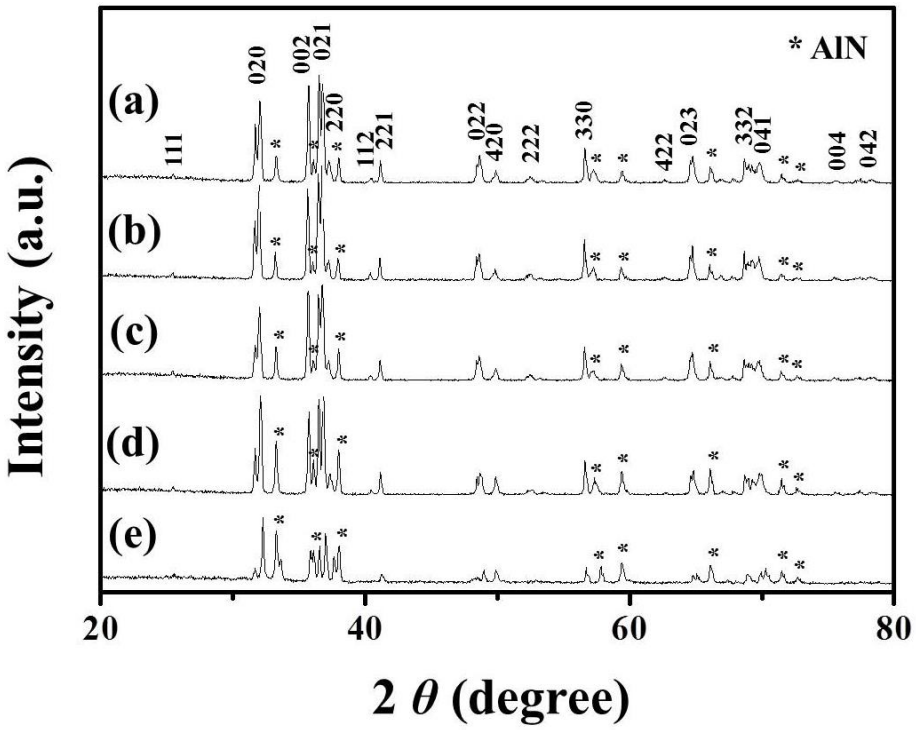

Fig. 3-2. XRD patterns of the $CaAlSiN_3:Eu^{2+}$(3 at%) phosphors prepared from the $CaCN_2/CaCO_3:Eu^{3+}$-based mixtures with various molar ratios of $CaCN_2$ and $CaCO_3:Eu^{3+}$: (a) 1.185 : 0, (b) 0.8325 : 0.3525, (c) 0.5925 : 0.5925, (d) 0.3525 : 0.8325, and (e) 0 : 1.185 (see Table 3-1).

Figure 3-3 shows the plotting of the AlN peak intensity and Ca contents (%). In case of molar ratio of $CaCN_2$ and $CaCO_3:Eu^{3+}$ (1.185 : 0)-based mixtures, the Ca content shows around 1.0 wt% with weak intensity of AlN. Without using with $CaCO_3:Eu^{3+}$ powder, large amount of molecular-carbon species were generating as a reductant source, but remaining as an impurity in the phosphor powder, so the emission intensity was weak although AlN peak intensity was low. On the other hand, $CaCN_2$ and $CaCO_3:Eu^{3+}$ (0 : 1.185)-based mixture shows the Ca content around 0.5 wt% with strong AlN peak intensity which was loosing of Ca content too large heating under the high temperature (>1600^{o}C). So the proper molar ratio of $CaCN_2$ and $CaCO_3:Eu^{3+}$ are required to optimize for prepare $CaAlSiN_3:Eu^{2+}$ phosphor.

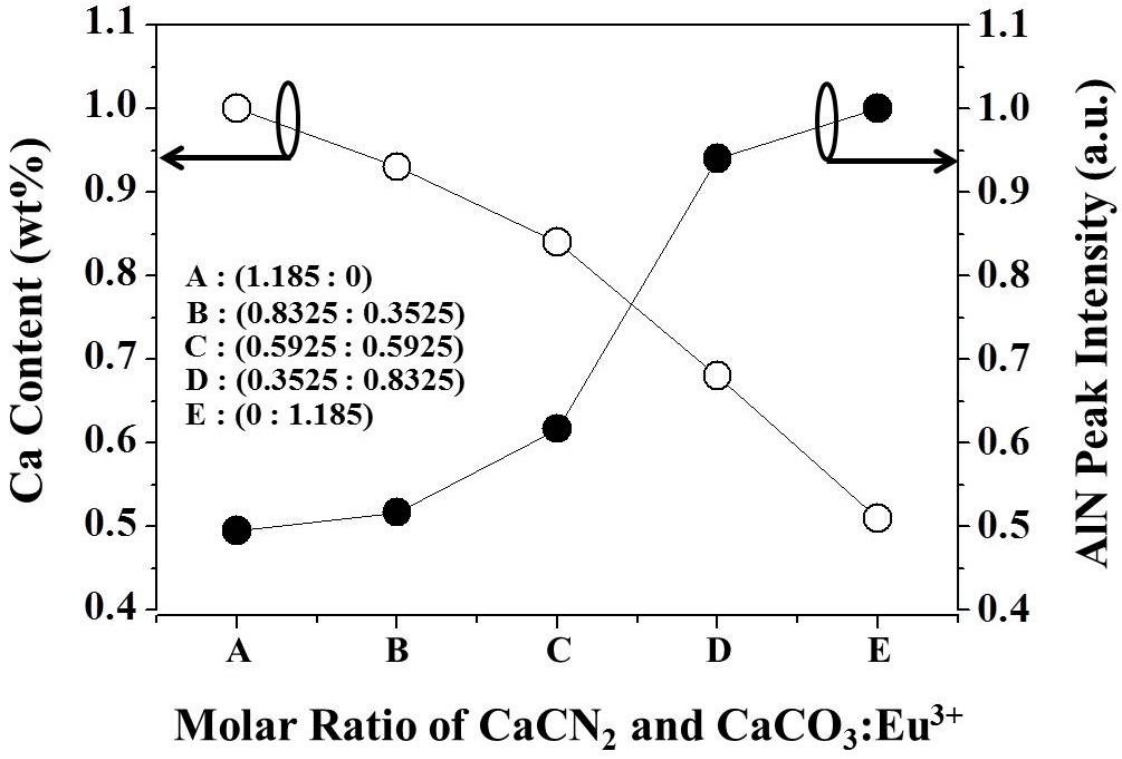

Fig. 3-3. Molar ratio dependences of $CaCN_2$ and $CaCO_3:Eu^{3+}$ on the AlN peak intensity and Ca content for the $CaAlSiN_3:Eu^{2+}$(3 at%) phosphors.

Figure 3-4 shows the excitation and emission spectra of $CaAlSiN_3:Eu^{2+}$ (3 at%) phosphors prepared with various molar ratios of $CaCN_2$ and $CaCO_3:Eu^{3+}$ measuring at the room temperature. The emission spectrum for sample (c) under an excitation of 450 nm has a broad band (FWHM ≈ 109 nm) ranging from 500 to 800 nm with a peak at 648 nm (red), which is attributed to the $4f^6 5d^1 \rightarrow 4f^7$ allowed transition of Eu^{2+} ion. The integrated emission intensity of sample (c) is about 89% of that of $YAG:Ce^{3+}$ (P46-Y3) and excitation spectrum shows the characteristic peak at the regions of 340-600 nm. The maximum excitation peaking at 450 nm was generally ascribed to the excitation of Eu^{2+} ion via the $4f^7 \rightarrow 4f^6 5d^1$ parity-allowed transition. The broad excitation band located at the ultraviolet to visible light area is suitable for phosphor-converted white LEDs fabricated with blue or ultraviolet LED chips as a light source [8-9, 14].

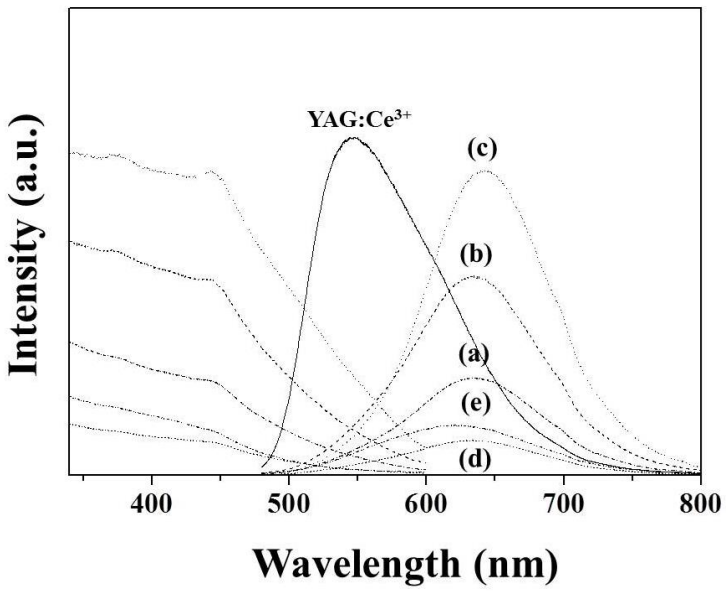

Fig. 3-4. PL spectra of the $CaAlSiN_3:Eu^{2+}$(3 at%) phosphors prepared from the $CaCN_2/CaCO_3:Eu^{3+}$-based mixtures with various molar ratios of $CaCN_2$ and $CaCO_3:Eu^{3+}$: (a) 1.185 : 0, (b) 0.8325 : 0.3525, (c) 0.5925 : 0.5925, (d) 0.3525 : 0.8325, and (e) 0 : 1.185 (see Table 3-1).

Table 3-1 shows the oxygen and nitrogen contents of the samples prepared from various molar ratios of $CaCN_2$ and $CaCO_3:Eu^{3+}$ mixture, together with their emission wavelength. Compared from sample (a) to (d), O/N values were much larger for the sample (e) which was prepared from without any use of reducing agent that shows poor reactivity resulting sample contained large amount of AlN.

Table 3-1. Oxygen/Nitrogen content and emission peak position (λ_{em}) of the $CaAlSiN_3:Eu^{2+}$(3 at%) phosphors prepared with different molar ratio of $CaCN_2$ and $CaCO_3:Eu^{3+}$ in raw materials

Sample	Molar ratio[a)] $CaCN_2:CaCO_3:Eu^{3+}$	Oxygen (wt%)	Nitrogen (wt%)	λ_{em} (nm)
(a)	1.185 : 0	2.05	15.56	633
(b)	0.8325 : 0.3525	2.12	17.24	633
(c)	0.5925 : 0.5925	1.75	20.54	648
(d)	0.3525 : 0.8325	2.54	23.89	633
(e)	0 : 1.185	17.47	26.17	621

[a)] Values for the excess amounts of $CaCN_2$ and $CaCO_3:Eu^{3+}$ to the raw material mixture with their stoichiometric ratio ($CaCN_2$: $CaCO_3:Eu^{3+}$: AlN : Si_3N_4 = 1 : 1 : 1 : 1/3).

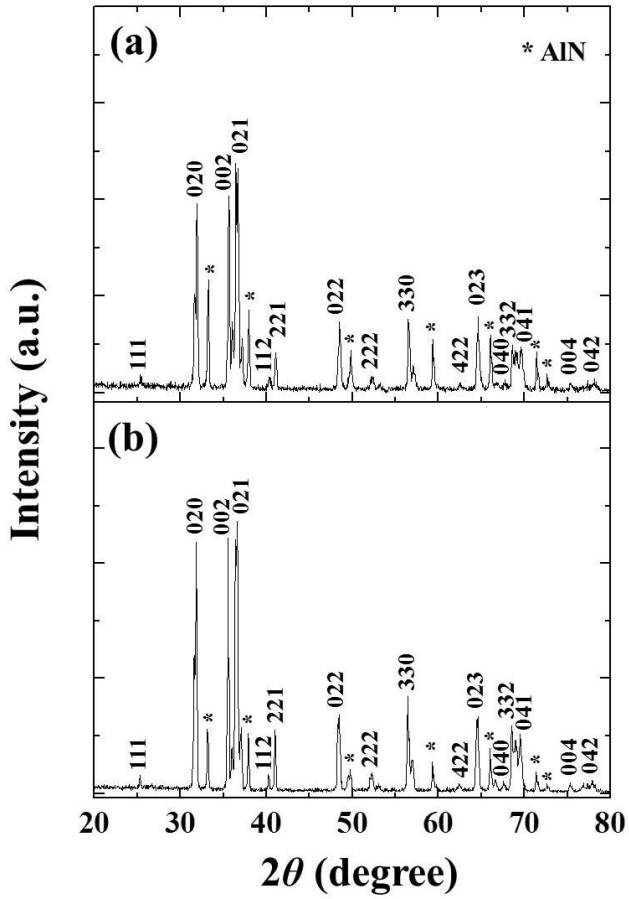

Fig. 3-5. XRD patterns of the $CaAlSiN_3:Eu^{2+}$(3 at%) phosphors prepared from raw material mixtures : (a) $CaCO_3:Eu^{3+}$, AlN, Si_3N_4, and C (molar ratio = 1.185 : 1: 1/3 : 1.185), and (b) $CaCN_2$, $CaCO_3:Eu^{3+}$, AlN, and Si_3N_4 (molar ratio = 0.5925 : 0.5925 : 1: 1/3).

Figure 3-5 shows the XRD patterns of $CaAlSiN_3:Eu^{2+}$(3 at%) phosphors prepared from $CaCO_3:Eu^{3+}$ reduced by C (a) and $CaCN_2$ (b). The XRD pattern (a) shows strong AlN peak intensity than that of pattern (b), which means that inorganic carbon species were very stable and no reduction at the high temperature (~1600^{o}C) compared with that of molecular carbon species ($^-$N=C=N$^-$) which was generating at 1150 - 1200^{o}C from the $CaCN_2$. Moreover, the oxygen content of the $CaAlSiN_3:Eu^{2+}$(3 at%) phosphor prepared from $CaCO_3:Eu^{3+}$ reduced by C (a) was very high (7.32 wt%) and relative emission intensity was too low (47 % of YAG:Ce^{3+}) with wavelength peaking at 644 nm. The reaction is quite insufficient than that of $CaAlSiN_3:Eu^{2+}$(3 at%) phosphor prepared from $CaCO_3:Eu^{3+}$ reduced by $CaCN_2$ (b).

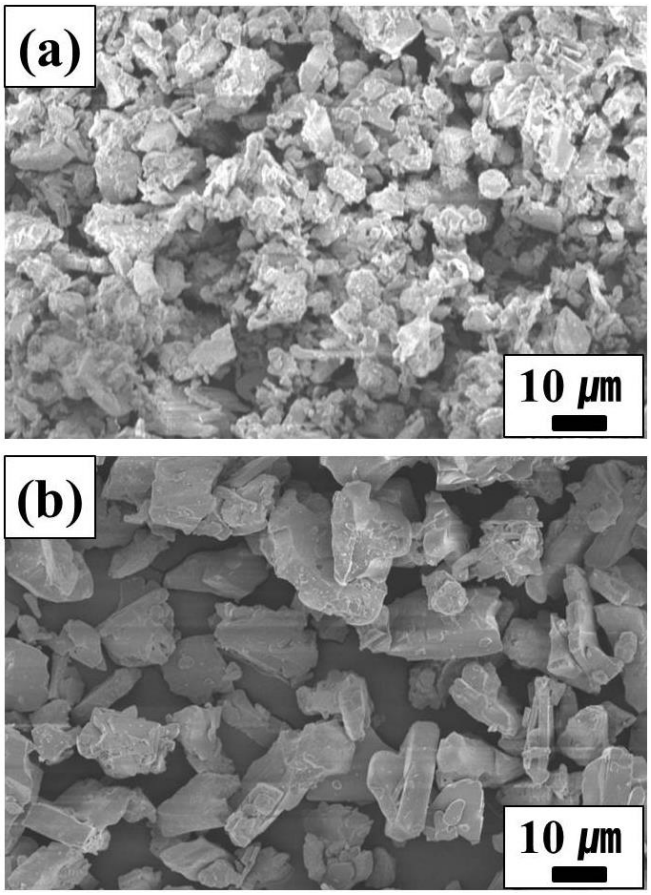

Fig. 3-6. SEM images of the $CaAlSiN_3:Eu^{2+}$(3 at%) phosphors given in Fig 5.

Figure 3-6 shows the typical SEM images for the $CaAlSiN_3:Eu^{2+}$(3 at%) phosphors prepared from the $CaCO_3:Eu^{3+}$ reduced by C (a) and $CaCN_2$ (b). The image (a) shows the cleavage planes of individual particles which were not smooth and other small particles were adhered to their surface. However, $CaAlSiN_3:Eu^{2+}$(3 at%) phosphors prepared by using proper amount of $CaCN_2$ powder (b), the observed surface of such cleavage planes became better smooth and the particles were facetted like single crystals with the mean size of about 20 μm.

Figure 3-7 shows the XRD patterns of the phosphors prepared from molar ratio of $CaCN_2$ and $CaCO_3:Eu^{3+}$ (0.5925 : 0.5925)-based mixture with changing *y*AlN contents (*y* = 1.0 - 0.6). All preparing conditions are completely assigned according to the cell data (JCPDS card: 39-0747), orthorhombic, $Cmc2_1$ (No.36), *a* = 9.740(1), *b* = 5.653(3), and *c* = 5.053(7) Å. The single phase of $CaAlSiN_3:Eu^{2+}$ phosphor was obtained below the *y*AlN content of 0.8, and those of atomic coordinates, isotropic displacement parameters are listed in Table 3-2.

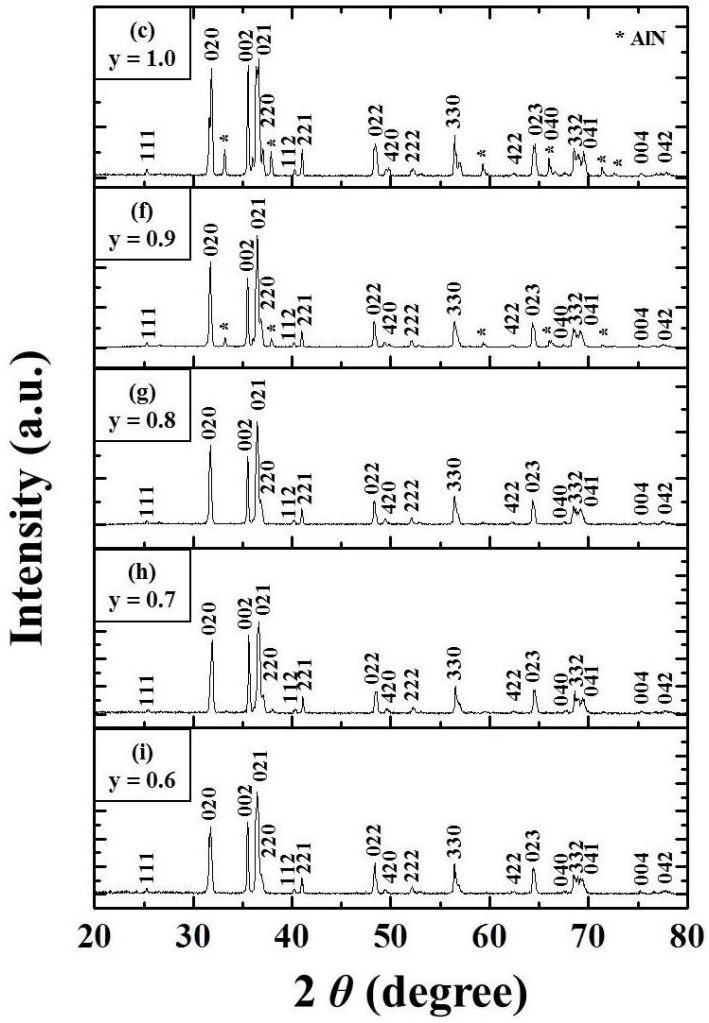

Fig. 3-7. XRD patterns of the $CaAlSiN_3:Eu^{2+}$(3 at%) phosphors prepared from the $CaCN_2/CaCO_3:Eu^{3+}$ (0.5925 : 0.5925)-based mixtures (see Table 3-1), where the AlN amount was changed from $y = 1$ to $y = 0.6 – 0.9$, respectively.

Table 3-2. Atomic coordinates and isotropic displacement parameters of the $CaAl_{0.8}SiN_3:Eu^{2+}$(3 at%) phosphor (sample c)

Atom	Site ($Cmc2_1$)	Coordinates[a)]			U_{iso} (Å^2)[a)]
		x	*y*	*z*	
Ca,Eu	4a	0	0.3141(1)	0.9747(6)	0.0169(7)
Al/Si	8b	0.1717(5)	0.8422(2)	0.0483(7)	0.0037(8)
N(1)	8b	0.2081(1)	0.8725(3)	0.4066(1)	0.0004(2)
N(2)	4a	0	0.2303(7)	0.5000(5)	0.0005(5)

[a)] R_p = 15.6 %, R_{wp} = 14.1 %, R_{exp} = 15.2 %.

Figure 3-8 shows the differential profile between the observed and calculated XRD patterns for the $CaAlSiN_3:Eu^{2+}$(3 at%) phosphor prepared from molar ratio of $CaCN_2$ and $CaCO_3:Eu^{3+}$ (0.5925 : 0.5925)-based mixture with *y*AlN (*y* = 0.8). One can see that the observed pattern is in good accordance with the calculated one due that the differential profile between these is so flat. This means that the $CaAlSiN_3:Eu^{2+}$ powders prepared from molar ratio of $CaCN_2$ and $CaCO_3:Eu^{3+}$ (0.5925 : 0.5925)-based mixture scarcely contain any impurity such as AlN (see Figs. 3-7).

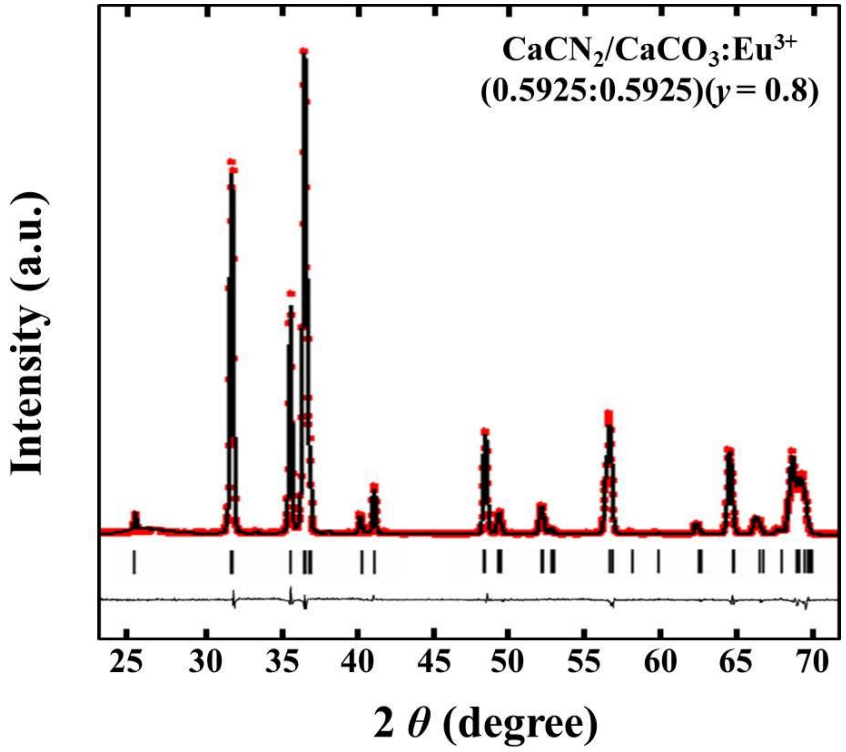

Fig. 3-8. Differential profile between the observed (circle) and calculated (line) XRD patterns for the $CaAlSiN_3:Eu^{2+}$(3 at%) phosphor prepared from prepared from the $CaCN_2/CaCO_3:Eu^{3+}$ (0.5925 : 0.5925)-based mixtures containing *y*AlN (*y* = 0.8) (see Fig. 7). The atomic coordinates and thermal parameters listed in Table 3-2 were used for calculating the peak intensity profile of XRD.

Table 3-3 shows summarize the analytical data of cationic ratios of the samples by measuring EDX analysis. Due to loss of Ca content fired at high temperature (~1600^{o}C), a Ca deficiency of 15% was observed for the stoichiometric starting composition of sample (c) prepared from a ratio

of Ca/Al/Si/Eu (1.185:1.00:1.00:0.03). By adjusting the AlN amount, optimized condition was obtained from starting composition of sample (g) prepared from a ratio of Ca/Al/Si/Eu (1.185:0.80:1.00:0.03).

Table 3-3. Analytical compositions and Luminescence properties of $CaAl_ySiN_3:Eu^{2+}$(3 at%) (y = 1.0 – 0.6) phosphors and their analytical O/N contents

	Analytical composition				λ_{em}	λ_{em}	R. I.	Oxygen	Nitrogen
y	Ca	Al	Si	Eu	(nm)	(nm)	(%)[a)]	(wt%)	(wt%)
(c) 1.0	0.85	1.14	0.85	0.03	450	648	89	1.7	20.5
(f) 0.9	0.91	1.09	0.90	0.03	450	654	93	1.3	22.4
(g) 0.8	1.01	0.98	1.01	0.03	450	654	102	0.7	24.5
(h) 0.7	1.02	0.87	1.12	0.03	450	648	75	3.1	23.4
(i) 0.6	1.03	0.81	1.18	0.03	450	648	70	4.7	22.1

[a)] The values were normalized by that of $YAG:Ce^{3+}$ (100%).

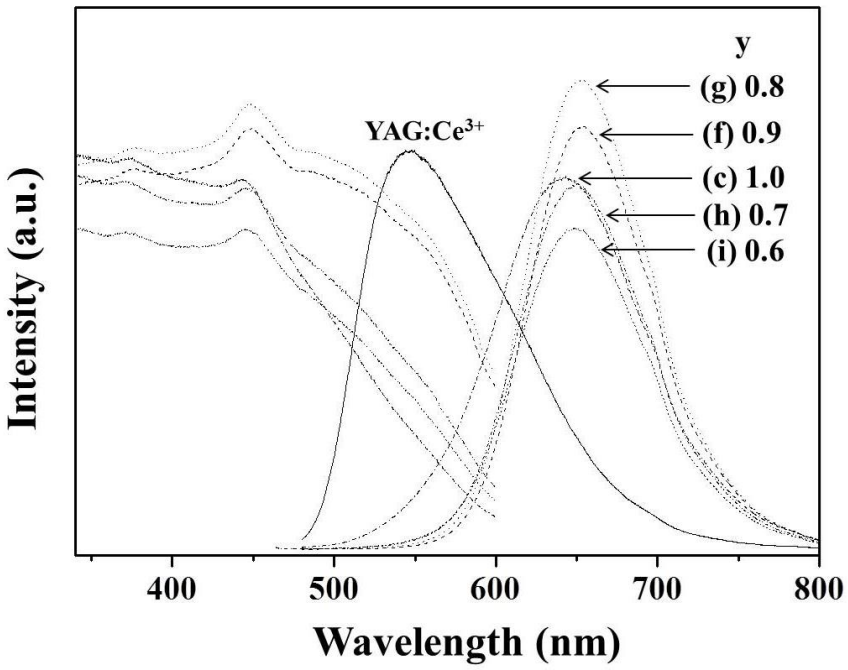

Fig. 3-9. PL spectra of the $CaAl_ySiN_3:Eu^{2+}$(3 at%) (y = 1.0 - 0.6) phosphors given in Fig. 7.

Figure 9 shows the PL spectra of the $CaAl_ySiN_3:Eu^{2+}$(3 at%) phosphors prepared from molar ratio of $CaCN_2$ and $CaCO_3:Eu^{3+}$ (0.5925 : 0.5925)-based mixture by changing of yAlN contents (y =

1.0 - 0.6). The obtained phosphor (y = 0.8) shows intense emission intensity compare with that of YAG:Ce^{3+}(P46-Y3) phosphor (102% of YAG:Ce^{3+}). When content of *y*AlN was decreased below 0.7, the emission intensity decreases due to lack of values of stoichiometric one. Their luminescence properties and oxygen/nitrogen contents are also shown in Table 3-3.

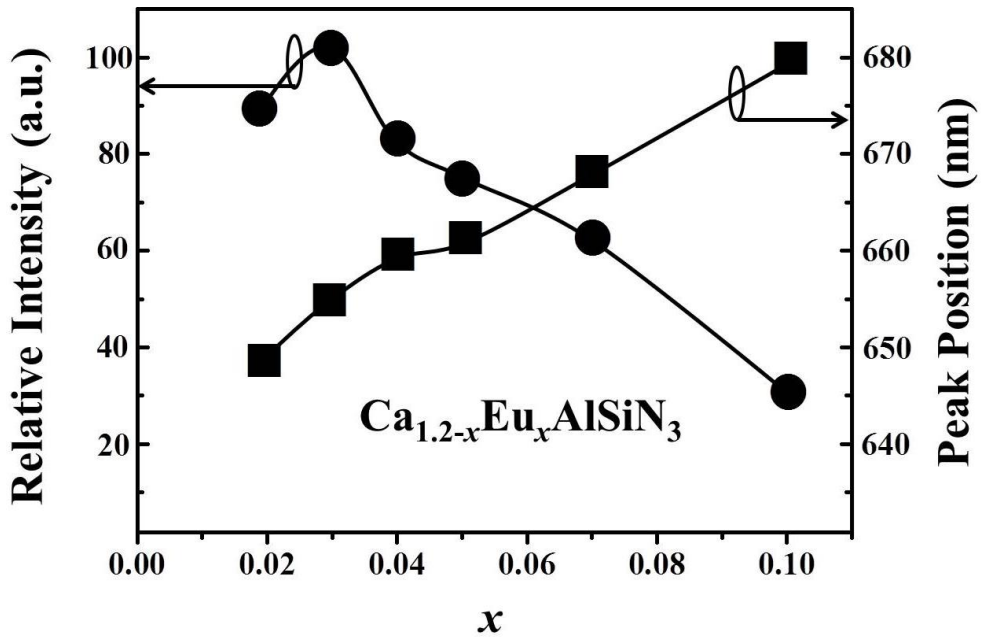

Fig. 3-10. Dependences of the Eu^{2+} concentration on the emission intensity and peak position of the $CaAlSiN_3$:Eu^{2+} phosphors prepared from molar ratios of $CaCN_2$ and $CaCO_3$:Eu^{3+} (0.5925 : 0.5925)-based mixtures containing 0.8 AlN, 1/3 Si_3N_4, and 0.005 - 0.05 Eu_2O_3.

Figure 3-10 shows the photoluminescence characteristics of the $(Ca_{1.2-x}Eu_x)AlSiN_3$ (x = 0.02 – 0.10) phosphors as a change in Eu^{2+} concentration. The emission intensity is supposed to be proportional to the activator amount in an ideal situation. However, there is always a critical concentration of activator, at which the emission intensity begins to decrease. This decrease can be ascribed by the concentration quenching which is mainly caused by a nonradiative energy transfer between two Eu^{2+} ions in the host lattice. In this work, with increasing Eu^{2+} ion content, the emission intensity is maximized at 3 at% of Eu^{2+} ion and then decreases slowly. At the same time, the emission peaks are shifted to the long wavelength when the Eu^{2+} concentration increases. This can be explained by the mismatch of ionic radius between the small Ca^{2+} and large Eu^{2+} in the

lattice [17]. The mismatch cause some changes in the crystal field and resulting in the splitting of 5*d* level of Eu^{2+}. So, possibility of energy transfer between higher 5*d* level and lower 5*d* level of Eu^{2+} ions may increase when the Eu concentration is increased. It is assumed that the high doping of Eu^{2+} ions reduces the emission energy, because the transition energy from higher 5*d* excited state to 4*f* ground state is larger than that of reverse case. Thus, the observed emission peak position of $Ca_{1.2-x}Eu_xAlSiN_3$ phosphors shifts from 648 to 679 nm by increasing the Eu^{2+} content.

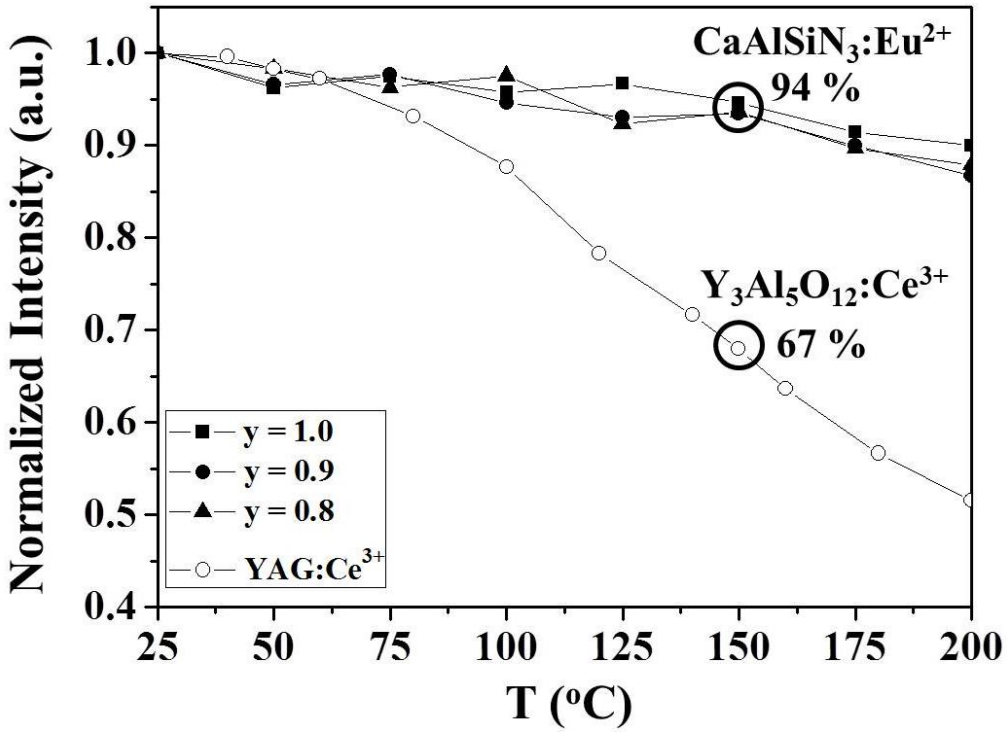

Fig. 3-11. Thermal quenching characteristics of the $CaAl_ySiN_3:Eu^{2+}$(3 at%) (y = 0.8, 0.9 and 1.0) phosphors prepared from molar ratios of $CaCN_2$ and $CaCO_3:Eu^{3+}$ (0.5925 : 0.5925)-based mixtures, together with that of $YAG:Ce^{3+}$ standard one.

Figure 3-11 shows the temperature dependence of the normalized PL intensity of $CaAl_ySiN_3:Eu^{2+}$ (y = 1.0 - 0.8) phosphor prepared from molar ratio of $CaCN_2$ and $CaCO_3:Eu^{3+}$ (0.5925 : 0.5925)-based mixture, compared with that of $YAG:Ce^{3+}$ (P46-Y3) phosphor. For the application of white LEDs, a temperature quenching behavior is one of the important parameters to evaluate the quality of a phosphor. When the temperature is increased to the working temperature of white LEDs (150°C), the emission intensity of $CaAl_ySiN_3:Eu^{2+}$ (3 at%) (y = 1.0 - 0.8) phosphors

against the excitation of 450 nm are about 94% of that at room temperature, respectively, and it is better than that of YAG:Ce^{3+} sample (68% at 150°C). The thermal quenching mechanism is commonly explained as an electronic transition between the $4f^6$-$5d^1$ and $4f^7$ states. From results of samples, $CaAl_ySiN_3:Eu^{2+}$(3 at%) (y = 1.0 - 0.8) phosphor has high quenching temperature and small Stokes shift of the Eu^{2+} ion in the rigid host. Thus, these phosphors are shown a low temperature quenching effect with high thermal stabilities.

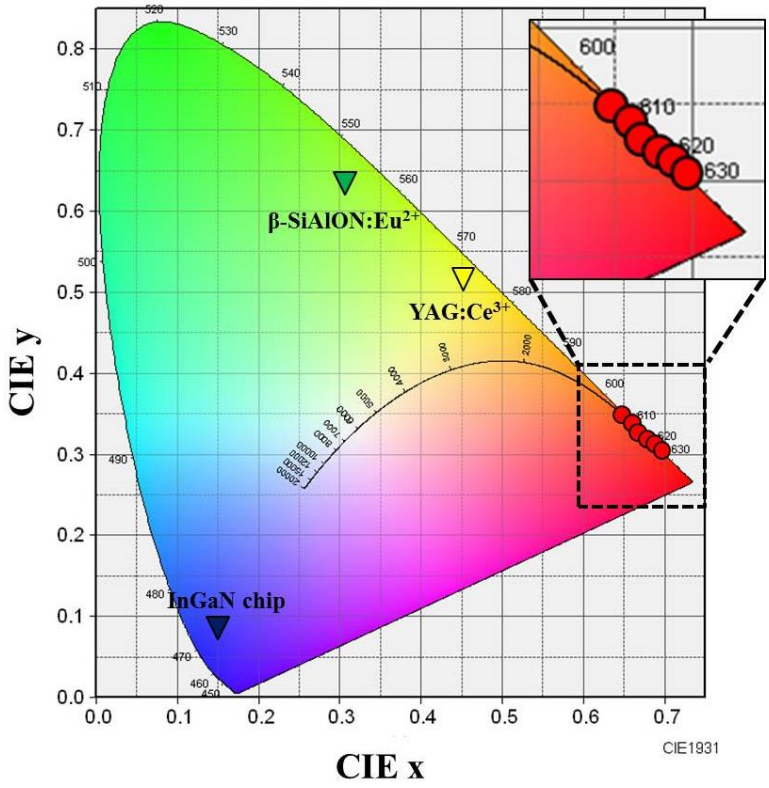

Fig. 3-12. CIE color coordinates for the $Ca_{1.2-x}Eu_xAlSiN_3$ phosphors doped with various amounts of Eu^{2+} (x = 0.01 - 0.1) prepared from molar ratios of $CaCN_2$ and $CaCO_3:Eu^{3+}$ (0.5925 : 0.5925)-based mixtures.

Figure 3-12 shows the Commission Internationale del'Eclairage (CIE) color coordinates of $Ca_{1.2-x}Eu_xAlSiN_3$ phosphors prepared from molar ratio of $CaCN_2$ and $CaCO_3:Eu^{3+}$ (0.585 : 0.585)-based mixture. Along with an increasing Eu^{2+} ion concentration, the chromaticity coordinates (x, y) shifts from (0.649, 0.349) to (0.691, 0.312) for $Ca_{1.2-x}Eu_xAlSiN_3$ (x = 0.02 - 0.10) while that of YAG:Ce^{3+} (P46-Y3) is measured to be (0.469, 0.533).

As indicated, the saturation of the chromaticity of the present $Ca_{1.2-x}Eu_xAlSiN_3$ (x = 0.02 - 0.10) phosphors were high enough to compensate for red color component and it is shown that the efficient white light with high color rendering index (CRI) value can possibly be made by combining with a blue LED chip together with a proper amount of green phosphor such as $MSi_2O_2N_2:Eu^{2+}$ (M = Ca, Sr, Ba) [18] or β-SiAlON:Eu^{2+} [19].

3.4 Conclusions

The high-quality red-emitting phosphor, $CaAlSiN_3:Eu^{2+}$ is synthesized from appropriate amount of $CaCN_2$ and $CaCO_3:Eu^{3+}$ mixture with optimized Al content. $CaCN_2$ is used as a source of Ca component as well as an effective reductant instead of carbon that is general inorganic reductant in the carbothermal reduction and nitridation method (CRN). Compared with the CRN method using the inorganic carbon powder, molecular carbon species are effectively used to synthesized of high-quality of $CaAlSiN_3:Eu^{2+}$(3 at%) phosphor, that is attributed to the unique chemical properties of $^-N=C=N^-$ groups in $CaCN_2$ (mp: 1340^{o}C and sp: Ca. 1175^{o}C [20]), indicating that the unreactive carbon residue is hardly formed.

The single phase of $CaAlSiN_3:Eu^{2+}$(3 at%) phosphor at the optimized concentration of 0.8 at% of Al gives the strongest emission intensity. These obtained phosphors are efficiently excited by the blue light (400 - 460 nm) of Ga(In)N-based LEDs, and the emission intensity is competitive with that of YAG:Ce^{3+} (P46-Y3) standard phosphor (*vs.* 102% of YAG:Ce^{3+}). Also, the $CaAlSiN_3:Eu^{2+}$ (3 at%) phosphors have a low thermal quenching effect which is useful for the high-brightness illumination application and the saturated chromaticity of the optimized samples indicates that these phosphors can be used as a red component for warm-white LEDs.

References

[1] R. J. Xie, N. Hirosaki, K. Sakuma, Y. Yamamoto and M. Mitomo, *Appl. Phys. Lett.*, **84**, 5404 (2004).

[2] N. Hirosaki, R.-J. Xie, K. Kimoto, T. Sekiguchi, Y. Yamamoto, T. Suehiro and M. Mitomo, *Appl. Phys. Lett.*, **86**, 211905 (2005).

[3] H. A. Höppe, H. Lutz, P. Morys, W. Schnick and A. Seilmeier, *J. Phys. Chem. Solid*, **61**, 2001

(2000).

[4] Y. Q. Li, J. E. J. van Steen, J. W. H. van Krevel, G. Botty, A. C. A. Delsing, F. J. DiSalvo, G. de With and H. T. Hintzen, *J. Alloys Compd.*, **417**, 273 (2006).

[5] X. Q. Piao, T. Horikawa, H. Hanzawa and K. Machida, *Appl. Phys. Lett.*, **88**, 161908 (2006).

[6] X. Q. Piao, T. Horikawa, H. Hanzawa and K. Machida, *Chem. Lett.*, **35**, 334 (2006).

[7] K. Uheda, H. Takizawa, T. Endo, H. Yamane, M. Shimada, C.-M. Wang and M. Mitomo, *J. Lumin.*, **967**, 87 (2000).

[8] X. Piao, K. Machida, T. Horikawa, H. Hanzawa, Y. Shimomura and N. Kijima, *Chem. Mater.*, **19**, 4592 (2007).

[9] K. Uheda, N. Hirosaki, Y. Yamamoto, A. Naito, T. Nakajima and H. Yamamoto, *Electrochem. Solid-State Lett.*, **9**, H22 (2006).

[10] K. Uheda, N. Hirosaki and H. Yamamoto, *Phys. Stat. Sol. (a)*, **203**, 2712 (2006).

[11] J. Li, T. Watanabe, N. Sakamoto, H. Wada, T. Setoyama and M. Yoshimura, *Chem. Mater.*, **20**, 2095 (2008).

[12] H. Watanabe, H. Wada, K. Seki, M. Itou and N. Kijima, *J. Electrochem. Soc.*, **155**, F31 (2008).

[13] J. Li, T. Watanabe, H. Wada, T. Setoyama and M. Yoshimura, *Chem. Mater.*, **19**, 3592 (2007).

[14] H. S. Kim, K. Machida, T. Horikawa and H. Hanzawa, *J. alloys compd.*, **633**, 97, (2015).

[15] X. Q. Piao, K. Machida, T. Horikawa and H. Hanzawa, *J. Rare. Earths.*, **26**, 198 (2008).

[16] H. S. Kim, K. Machida, T. Horikawa and H. Hanzawa, *Chem. Lett.*, **43**, 533 (2014).

[17] R. D. Shannon, *Acta Crystallogr. Sect. A: Cryst. Phys. Diffr. Theor. Gen. Crystallogr.*, **32**, 751 (1975).

[18] Y. -Q. Li, A. C. A. Delsing, G. de With and H. T. Hintzen, *Chem. Mater.*, **17**, 3242 (2005).

[19] H. Wu, X. M. Zhang, C. F. Guo, J. Xu, M. M. Wu, Q. Su, *IEEE Photon. Technol. Lett.*, **17** (2005) 1160.

[20] P. Patnaik, *Handbook of Inorganic Chemicals*, McGrawHill, New York, (2002).

Chapter 4

Summary

In the present work, some efficient process for producing the $CaAlSiN_3:Eu^{2+}$ and $(Sr,Ca)AlSiN_3:Eu^{2+}$ phosphors (Self-propagating High-temperature Synthesis/SHS and Carbothermal Reduction and Nitriding/CRN) were developed by using the fine powders of hydrides, $(Ca,Eu)AlSiH_x$ and $(Sr,CaEu)AlSiH_x$, the powder mixtures of $CaCO_3:Eu^{3+}$ and $Ca(CH_3COO)_2$ or $CaCN_2$, AlN, and Si_3N_4, respectively. Futhermore, the resultant phosphors were characterized on the basis of structural, compositional, and grain morphological analyses and luminescence spectral measurements to evaluate the possibility of their practical use as the white LEDs for display backlight and general illumination lamps.

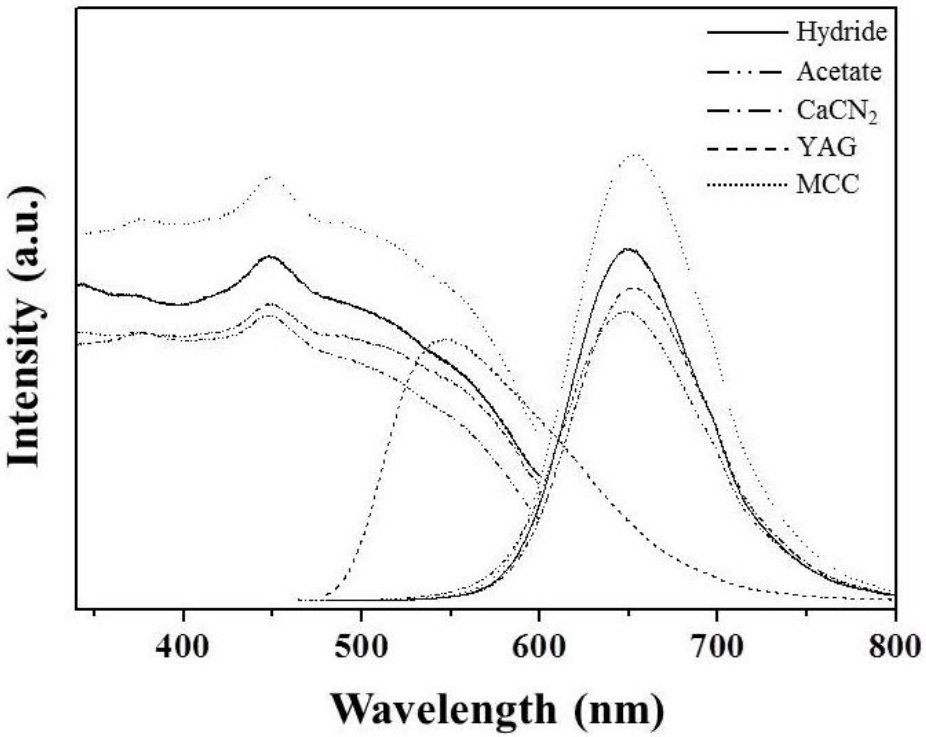

Fig. 4-1. Luminescence spectra of the $CaAlSiN_3:Eu^{2+}$ phosphors prepared from SHS and CRN processes, together with those of commercially available $YAG:Ce^{3+}$ (P46-Y3) and $CaAlSiN_3:Eu^{2+}$ phosphors as the references, which were offered by Mitsubishi Chemical Co.Ltd.

For the SHS process, the $CaAlSiN_3:Eu^{2+}$ and $(Sr,Ca)AlSiN_3:Eu^{2+}$ phosphors were produced as the single phase without any impurities by adding an excess amount of CaH_2 powder to each starting material of $(Ca,Eu)AlSiH_x$ or $(Sr,Ca,Eu)AlSiH_x$. The SHS reaction took place uniformely and the resultant phosphors gave the intense red emissions in the range of 635–650 nm (see Fig.4-1 and Table 4-1), which were noted to be practically usable as the red phosphor for the white LEDs.

Table 4-1. Comparison of oxygen, carbon contents, and relative emission intensity of the resultant phosphors

Phosphor	Starting Materials	Oxygen (wt%)	Peak position (nm)	R.I. (%)[c]
$CaAlSiN_3:Eu^{2+}$	$CaCO_3$ + C (Graphite)[a]	7.32	644	47
	$Ca(HCOO)_2$ + C (Vapor)[a]	0.89	650	67
	$Ca(CH_3COO)_2$ + C(Vapor)[a]	0.71	650	93
	$CaCN_2$ + $CaCO_3$[a]	0.70	654	102
	CaAlSi[b]	4.21	644	63
	$CaAlSiH_x$[b]	0.72	650	110
$(Sr_{0.54}Ca_{0.44})AlSiN_3:Eu^{2+}$	$(Sr,Ca)AlSiH_x$[b]	0.82	635	78
$(Sr_{0.42}Ca_{0.56})AlSiN_3:Eu^{2+}$	$(Sr,Ca)AlSiH_x$[b]	0.79	644	90
$YAG:Ce^{3+}$ (P46-Y3)	-	-	544	100
$CaAlSiN_3:Eu^{2+}$ (MCC)[d]	-	-	654	140

[a] Carbothermal reduction and nitridation method (CRN).

[b] Self-propagating High-temperature Synthesis (SHS).

[c] The values were normalized by the basis of that of $YAG:Ce^{3+}$ (100%).

[d] The sample is offered by Mitsubishi Chemical Co.Ltd.

The developed CRN methods using $Ca(CH_3COO)_2$ and $CaCN_2$ were also found to be the efficient processes for producing high-quality powders of $CaAlSiN_3:Eu^{2+}$ phosphor at the low cost comparing with the conventional solid-state reaction method using Ca_3N_2, EuN, AlN, and Si_3N_4 powders as the raw materials. In particular, even though carbonaceous materials such as $Ca(CH_3COO)_2$ and $CaCN_2$ were used as the main raw materials, the carbon impurity, which depressed the emission intensity, was very low (<0.5 at%). This is due that the carbon species of them, CH_3COO^- and CN^-, are volatile as well as playing as the reductant to convert from $CaCO_3$ (or CaO) to Ca_3N_2, so that the unreacted portions of them should go out from the samples at the higher temperature for heating. The luminescence properties of the resultant $CaAlSiN_3:Eu^{2+}$

phosphors are given in Fig. 4-1 and Table 4-1, together with the commercially available YAG:Ce^{3+} and $CaAlSiN_3:Eu^{2+}$ phosphors as the references.

The author believes that findings and results obtained in this work will contribute to the academic and industrial researches for nitride phosphor synthesis.

List of Publications

1. Carbothermal Reduction Synthesis using $CaCN_2$ as Calcium and Carbon Source for $CaAlSiN_3:Eu^{2+}$ Phosphor and Their Luminescence Properties

Hyo Sung Kim, Ken-ichi Machida, Takashi Horikawa, Hiromasa Hanzawa

Chem. Lett., **9** (2013) 131050.

2. Synthesis and Luminescence Properties of $(Sr,Ca)AlSiN_3:Eu^{2+}$ Phosphors under Atmospheric-Pressure

Hyo Sung Kim, Ken-ichi Machida, Masahiro Itoh, Hiromasa Hanzawa

ECS J. Solid State Sci. and Tech., **3** (2014) R234.

3. Luminescence Properties of $CaAlSiN_3:Eu^{2+}$ Phosphor Prepared by Direct-nitriding Method using Metal Hydride Fine Powders

Hyo Sung Kim, Ken-ichi Machida, Takashi Horikawa, Hiromasa Hanzawa

J. Alloys and Compd., **633** (2015) 97-103.

4. Synthesis of $CaAlSiN_3:Eu^{2+}$ Phosphor by CRN Method and Their Luminescent Properties for White-LEDs

Hyo Sung Kim, Ken-ichi Machida, Takashi Horikawa, Hiromasa Hanzawa

ECS J. Solid State Sci. and Tech., in contribution.

5. Carbothermal Reduction Characteristics of Calcium Formate and Acetate for Producing $CaAlSiN_3:Eu^{2+}$ Phosphor

Hyo Sung Kim, Ken-ichi Machida, Hiromasa Hanzawa

J. Alloys and Compd., in contribution.

Acknowledgements

This Ph. D. work has been carried out from Oct. 2010 to Apr. 2015 in Division of Applied Chemistry, Graduate School of Engineering, Osaka University. Firstly, I would like to express my sincere gratitude to my advisor Prof. Dr. Ken-ichi Machida for his kind guidance, valuable suggestion, and support throughout this work. He has been encouraging me to investigate the topic of this work which I found very interesting.

I am deeply grateful to Prof. Dr. Nobuhito Imanaka at Division of Applied Chemistry and Prof. Dr. Yasufumi Fujiwara at Division of Materials and Manufacturing Science, Graduate School of Engineering of Osaka University for reviewing this thesis and giving their valuable comments.

I would like to thank Dr. Hiromasa Hanzawa and Dr. Takashi Horikawa for their great contributions in the setup and maintenance of the experimental instruments and photoluminescence measurement system for nitride phosphors as well as valuable advice about this work. I would like to acknowledge Dr. Masahiro Itoh for his continuous encouragement as well as helpful discussion.

I would like to thank Dr. Yasuo Shimomura (Mitsubishi chemical Co. Ltd., Science & Technology Research Center) for valuable comments and also thank to Prof. Dr. Hyoun-Woo Kim at Division of Materials Science and Engineering, Hanyang University.

Special thanks should be given to all the members of the research group under the direction of Prof. Ken-ichi Machida at Osaka University for their friendships and kindness. Whenever I asked for a help, they always meet my requirement without any hesitations.

Finally, I would like to thank to my parents Mr. Myeong-Wook Kim and Mrs. Sun-Ja Kim, my younger sister Mrs. Da-Young Kim and her husband Mr. Jun-Gi Park and my all relatives for their hearty encouragements, continuous understanding, and perpetual supports.